Journal of Medicinal Chemistry

Article

Discovery of 4-Methyl-N-(4-((4-methylpiperazin-1-yl)methyl)-3-(trifluoromethyl) phenyl)-3-((1-nicotinoylpiperidin-4-yl)oxy)benzamide (CHMFL-ABL/KIT-155) as a Novel Highly Potent Type II ABL/ KIT Dual Kinase Inhibitor with a Distinct Hinge Binding

Qiang Wang, Feiyang Liu, Beilei Wang, Fengming Zou, Ziping Qi, Cheng Chen, Kailin Yu, Chen Hu, Shuang Qi, Wenchao Wang, Zhenquan Hu, Juan Liu, Wei Wang, Li Wang, Qianmao Liang, Shanchun Zhang, Tao Ren, Qingsong Liu, and Jing Liu

J. Med. Chem., **Just Accepted Manuscript** • DOI: 10.1021/acs.jmedchem.6b01290 • Publication Date (Web): 30 Nov 2016

Discovery of 4-Methyl-*N*-(4-((4-methylpiperazin-1-yl)methyl)-3-(trifluoromethyl) phenyl)-3-((1-nicotinoylpiperidin-4-yl)oxy)benzamide (CHMFL-ABL/KIT-155) as a Novel Highly Potent Type II ABL/KIT Dual Kinase Inhibitor with a Distinct Hinge Binding

Qiang Wang[1,2,6], Feiyang Liu[1,3,6], Beilei Wang[1,3,6], Fengming Zou[1,2,6], Ziping Qi[1,2], Cheng Chen[1,3], Kailin Yu[1,3], Chen Hu[1,3], Shuang Qi[1,2], Wenchao Wang[1,2], Zhenquan Hu[1,2], Juan Liu[1], Wei Wang[1,2], Li Wang[1,3], Qianmao Liang[1], Shanchun Zhang[2,4], Tao Ren[5], Qingsong Liu[1,2,3,5], Jing Liu[1,2]**

1. High Magnetic Field Laboratory, Chinese Academy of Sciences, Mailbox 1110, 350 Shushanhu Road, Hefei, Anhui 230031, P. R. China
2. CHMFL-HCMTC Target Therapy Joint Laboratory, 350 Shushanhu Road, Hefei Anhui 230031, P. R. China
3. University of Science and Technology of China, Hefei, Anhui 230036, P. R. China
4. Hefei Cosource Medicine Technology Co. LTD., 358 Ganquan Road, Hefei, Anhui 230031, P. R. China

5. Precision Targeted Therapy Discovery Center, Institute of Technology Innovation, Hefei Institutes of Physical Science, Chinese Academy of Sciences, Hefei, Anhui 230088, P. R. China

6. These authors contribute equally

ABSTRACT

The discovery of a novel potent type II ABL/c-KIT dual kinase inhibitor compound **34** (CHMFL-ABL/KIT-155), which utilized a hydrogen bond formed by NH on the kinase backbone and carbonyl oxygen of **34** as a unique hinge binding, is described. **34** potently inhibited purified ABL (IC_{50}: 46 nM) and c-KIT kinase (IC_{50}: 75 nM) in the biochemical assays and displayed high selectivity (S Score (1) = 0.03) at the concentration of 1 μM among 468 kinases/mutants in KINOMEscan assay. It exhibited strong anti-proliferative activities against BCR-ABL/c-KIT driven CML/GISTs cancer cell lines through blockage of the BCR-ABL/c-KIT mediated signaling pathways, arresting cell cycle progression and induction of apoptosis. **34** possessed a good oral PK property and effectively suppressed the tumor progression in the K562 (CML) and GIST-T1 (GISTs) cells mediated xenograft mouse model. The distinct hinge-binding mode of **34** provided a novel pharmacophore for expanding the chemical structure diversity for the type II kinase inhibitors discovery.

INTRODUCTION

Type II kinase inhibitors that are featured by binding to the "DFG-out" inactive conformation of the kinases are an important class of drugs for anti-cancer therapy. Currently among over 30 FDA approved kinase inhibitors, at least 7 of them, such as **1** (Imatinib, Figure 1),[1] **2** (Sorafenib),[2] **3** (Nilotinib),[3] **4** (Regorafenib),[4] **5** (Cabozantinib),[5] **6** (Ponatinib),[6] and **7**

(Lenvatinib),[7] are believed to exert their functions through type II binding mode.[8, 9] In the canonical DFG-out binding mode, type II kinase inhibitors usually share similar structural features, including a moiety forming a hydrogen bond at the hinge-binding site, a moiety (usually an amide, urea, or 1,3-diketone) providing two hydrogen bonds with the Glu in the c-Helix and the Asp in the DFG motif, as well as a hydrophobic tail accommodating the hydrophobic pocket formed upon "DFG-out" shift.[9] As shown in Figure 1, the chemical structures that provide the two hydrogen bonds and the hydrophobic tails are diverse, while the hinge-binding moieties seem to be quite conservative, *e. g.* the *N*-heteroaromatic rings in compounds **1**-**7**. There are a few exceptions, such as p38/Eph inhibitor **8** (BIRB796),[10] **9** (PDK1 inhibitor MP7)[11] and DDR1 inhibitor **10** (DDR1-IN-1)[12] that bear unusual hinge binding hydrogen bond donors, *i. e.*, the oxygen of morpholine, the oxygen of benzene-fused urea and the oxygen of cyclic amide, which have been demonstrated in the X-ray crystal structures. The hydrogen bond between the hinge-binding moieties of type II inhibitors and the specific amino acid residues in the kinase backbone hinge region is crucial and required for the inhibitory potency. Given the fact that the chemical diversity of the middle part and the hydrophobic tail have been extensively explored while the hydrogen bond formation mode in the hinge binding part is relatively less investigated, seeking for new hinge binding mode will help to expand the pharmacophore diversity of type II inhibitors, which will lead to the discovery of more novel type II kinase inhibitors.

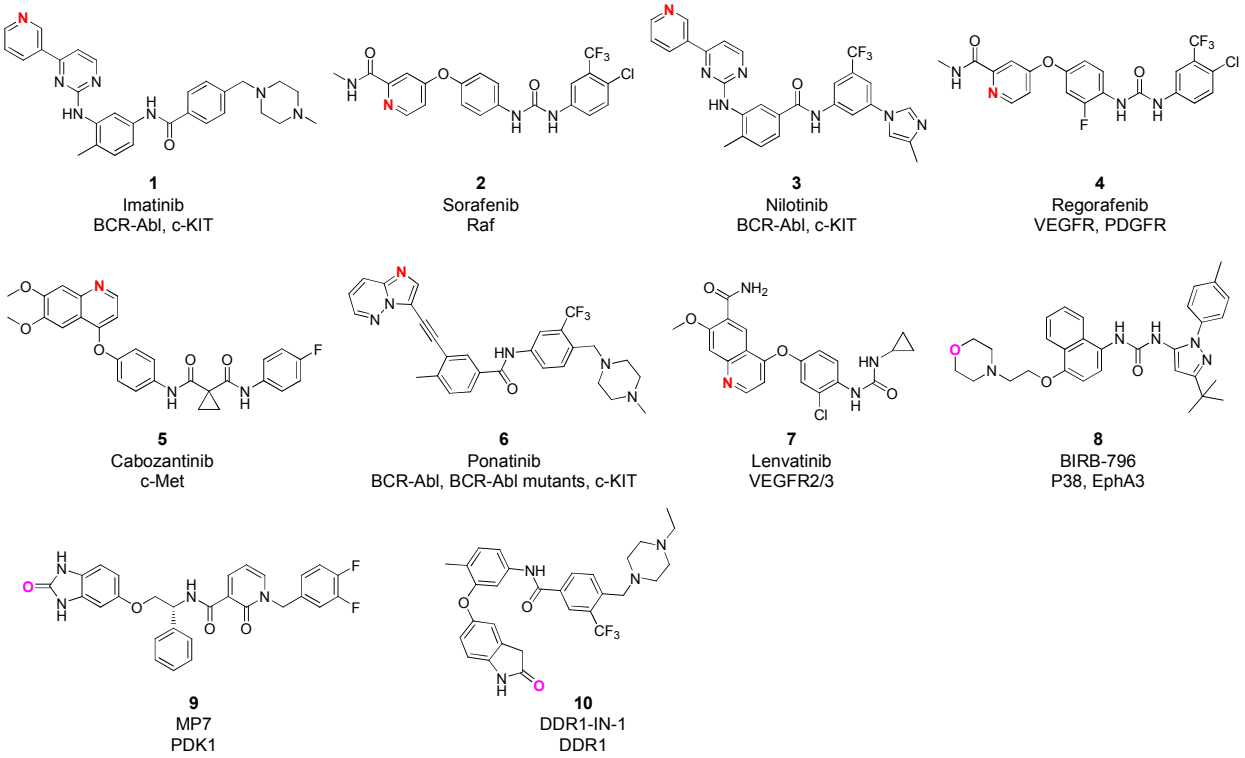

Figure 1. Representative type II inhibitors with nitrogen-mediated hinge binding (**1-7**) and distinct oxygen-mediated hinge binding (**8-10**).

Recently, we reported a potent type II ABL/PDGFR inhibitor **12** (CHMFL-074), which displayed a distinct hinge binding hydrogen bond formed by oxygen of amide in **12** and NH of amide on the ABL kinase backbone in the X-ray crystal structure (PDB ID: 5HU9).[13] This encouraged us to explore extensively of this novel pharmarcophore. Through a structure guided drug design approach, the medicinal chemistry effort led to the discovery of a potent type II ABL/c-KIT dual kinase inhibitor compound **34** (CHMFL-ABL/KIT-155), which exhibited a suitable biochemical and PK/PD profile in the in vitro and in vivo disease models of CML as well as GISTs.

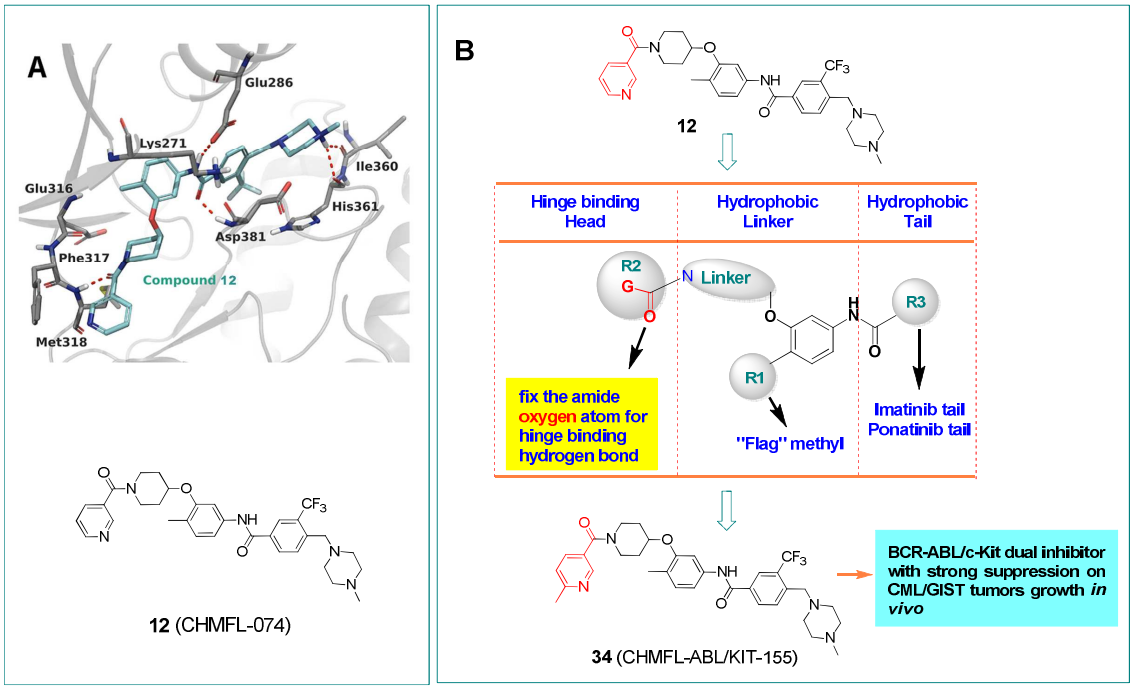

Figure 2. Schematic illustration of discovery of compound **34** with distinct hinge binding. (A) X-ray co-crystal structure of compound **12** with ABL kinase (PDB ID: 5HU9). (B) Structure-activity relationship (SAR) investigation route leading to compound **34** (CHMFL-ABL/KIT-155).

RESULTS AND DISCUSSION

Chemistry and Structure-Activity Relation (SAR) Investigation

As depicted in Figure 2B, compounds **11-39** were prepared following the synthetic route shown in Scheme 1 and Scheme 2.

The synthesis of compounds **11** and **12** began from nucleophilic substitution reaction between **40a** and *tert*-butyl 4-((methylsulfonyl)oxy)piperidine-1-carboxylate which provided **41a** (Scheme 1). After deprotection of the Boc group under acidic condition, subsequent amide coupling reaction with nicotinic acid afforded **43g**. Then hydrogenation of the nitro group

followed by amide coupling reaction with corresponding benzoic acid derivatives furnished the final products **11** and **12** respectively.

Scheme 1. Synthesis of Compounds 11 and 12[a]

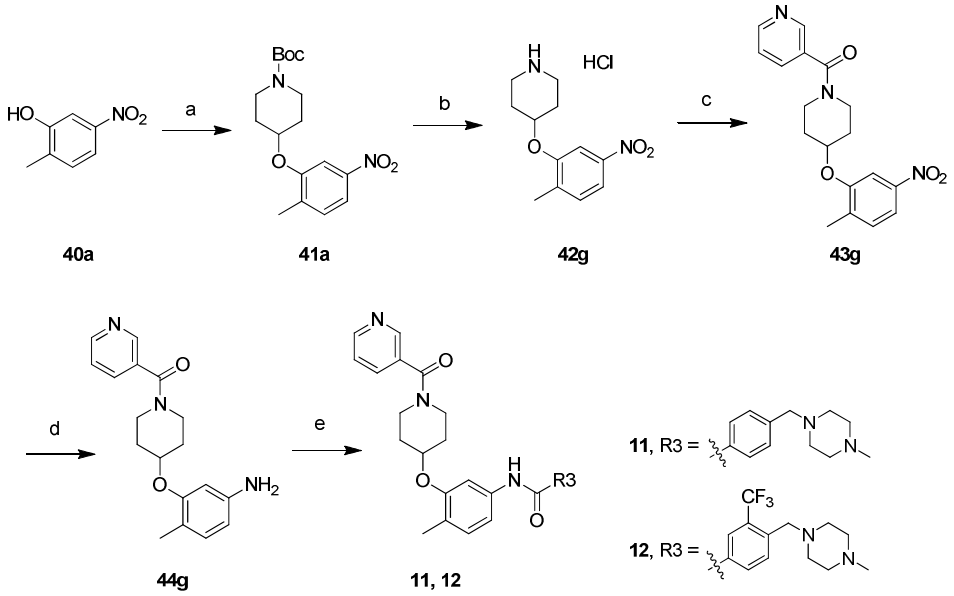

[a]Reagents and conditions: (a) *tert*-butyl 4-((methylsulfonyl)oxy)piperidine-1-carboxylate, K_2CO_3, DMF, 90 °C, overnight; (b) 4 N HCl in EtOAc, rt, overnight; (c) nicotinic acid, HATU, DIPEA, DMF, rt, 2 h; (d) H_2, Pd/C, EtOAc, rt, 6 h; (e) R3-COOH, HATU, DIPEA, DMF, rt, 2h.

Compounds **13-39** were obtained following a five-step synthetic route (Scheme 2). Starting from R1 substituted nitrophenol analogs **40a-c**, a nucleophilic substitution reaction with Boc protected amines afforded **41a-f**. Reduction of the nitro group to amino group via Palladium catalyzed hydrogenation followed by amide coupling reaction with the benzoic acid derivative offered **43a-f.** Removal of the Boc protection under acidic condition followed by amide coupling with varieties of carboxylic acids or nucleophilic substitution with different electrophiles provided desired compounds **13-39**.

Scheme 2. Synthesis of Compounds 13-39[a]

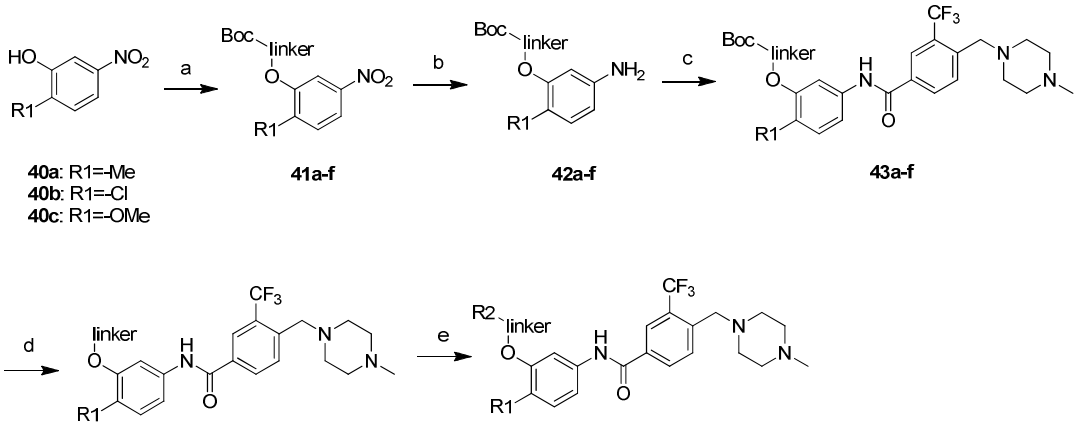

40a: R1=-Me
40b: R1=-Cl
40c: R1=-OMe

41a-f **42a-f** **43a-f**

44a-f

41a-44a: R1=-Me, linker=-4-piperidine
41b-44b: R1=-Me, linker=-3-methylpyrrolidine
41c-44c: R1=-Me, linker=-3-methylazetidine
41d-44d: R1=-Me, linker=-ethanamine
41e-44e: R1=-Cl, linker=-4-piperidine
41f-44f: R1=-OMe, linker=-4-piperidine

13-39

13: R1=-Me, linker=-ethanamine, R2=nicotinoyl
14: R1=-Me, linker=-3-methylpyrrolidine, R2=nicotinoyl
15: R1=-Me, linker=-3-methylazetidine, R2=nicotinoyl
16: R1=-Cl, linker=-4-piperidine, R2=nicotinoyl
17: R1=-OMe, linker=-4-piperidine, R2=nicotinoyl
18: R1= -Me, linker=-4-piperidine, R2= pyridine-3-acetyl
19: R1= -Me, linker=-4-piperidine, R2= propionyl
20: R1= -Me, linker=-4-piperidine, R2= acryloyl
21: R1= -Me, linker=-4-piperidine, R2= 2-(dimethylamino)acetyl
22: R1= -Me, linker=-4-piperidine, R2= benzoyl
23: R1= -Me, linker=-4-piperidine, R2= picolinoyl
24: R1= -Me, linker=-4-piperidine, R2= isonicotinoyl
25: R1= -Me, linker=-4-piperidine, R2= thiophene-3-carbonyl
26: R1= -Me, linker=-4-piperidine, R2= furan-3-carbonyl
27: R1= -Me, linker=-4-piperidine, R2= quinoline-3-carbonyl
28: R1= -Me, linker=-4-piperidine, R2= 2-fluoronicotinoyl
29: R1= -Me, linker=-4-piperidine, R2= 5-chloronicotinoyl
30: R1= -Me, linker=-4-piperidine, R2= 2-chloronicotinoyl
31: R1= -Me, linker=-4-piperidine, R2= 2-methylnicotinoyl
32: R1= -Me, linker=-4-piperidine, R2= 4-methylnicotinoyl
33: R1= -Me, linker=-4-piperidine, R2= 5-methylnicotinoyl
34: R1= -Me, linker=-4-piperidine, R2= 6-methylnicotinoyl
35: R1= -Me, linker=-4-piperidine, R2= 6-oxo-1,6-dihydropyridine-3-carbonyl
36: R1= -Me, linker=-4-piperidine, R2= 2-aminopyrimidine-5-carbonyl
37: R1= -Me, linker=-4-piperidine, R2= benzenesulfonyl
38: R1= -Me, linker=-4-piperidine, R2= 6,7-dimethoxy-4-methylquinazoline
39: R1= -Me, linker=-4-piperidine, R2=-2-pyrimidine

[a]Reagents and conditions: (a) for **41a**, **e-f**: *tert*-butyl 4-((methylsulfonyl)oxy)piperidine-1-carboxylate, for **41b**: *tert*-butyl 3-(((methylsulfonyl)oxy)methyl)pyrrolidine-1-carboxylate, for **41c**: *tert*-butyl 3-(((methylsulfonyl)oxy)methyl) azetidine-1-carboxylate, for **41d**: *tert*-butyl (2-bromoethyl)carbamate, K_2CO_3, DMF, 90 ^oC, overnight; (b) H_2, Pd/C, EtOAc, rt, 6 h; (c) 4-((4-methylpiperazin-1-yl)methyl)-3-(trifluoromethyl) benzoic acid, HATU, DIPEA, DMF, rt, 2 h; (d) 4 N HCl in EtOAc, rt, overnight; (e) for **13-36**: carboxylic acid derivatives, HATU, DIPEA, DMF, rt, 2 h; for **37**: benzenesulfonyl chloride, DIPEA, DMF, rt, 2 h; for **38**: 4-chloro-6,7-

dimethoxyquinazoline and for **39**: 2-chloropyrimidine, DIPEA, *n*-butyl alcohol, reflux, overnight.

BCR-ABL driven BaF3 based isogenic P210-BaF3 cell and c-KIT dependent TEL-c-KIT BaF3 cell were used to examine the SAR of the newly generated compounds by testing cell's growth inhibition (GI_{50s}) as the readout. We first fixed the hinge binding (R2) part as nicotinamide and varied the linker, R1 and R3 moieties (Table 1). Compared to compound **1**, replacement of the pyrimidine with piperidine ring in the linker part (**11**) lost potencies both to ABL and c-KIT kinases. However, compound **12** that possessed compound **6**'s tail gained desirable potencies against P210-BaF3 and TEL-c-KIT BaF3 cell lines. Therefore, the tail part (R3) was retained. For the subsequent optimization, we mainly focused on the linker, the flag methyl and the hinge binding moieties. With the tail (R3), flag methyl (R1) and the head fixed, we firstly investigated the linker moiety. Changing the linker from piperidine to ethanamine (**13**), 3-methylpyrrolidine (**14**) and 3-methylazetidine (**15**) all resulted in significant activity loss. In addition, compounds **14** and **15** started to gain activity to IL-3 dependent parental-BaF3 cell line. The data showed that a chloro atom at R1 position (**16**) displayed a similar trend to methyl group (**12**) in activities, while a bulky methoxy group (**17**) lowered the potency against both ABL and c-KIT kinases.

Table 1. SAR Exploration Focused on the R1/R3/linker moieties[a]

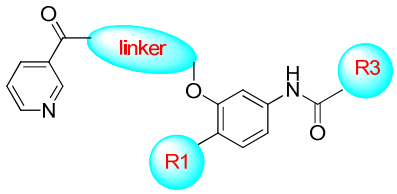

Compd	R1	linker	R3	P210-BaF3 (GI_{50}: μM)	Tel-c-KIT BaF3 (GI_{50}: μM)	WT-BaF3 (GI_{50}: μM)
1	-	-	-	0.27±0.001	0.37±0.031	>10
11	-Me	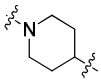	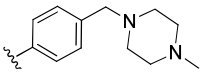	8.78±1.25	>5	>10
12	-Me	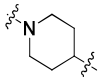	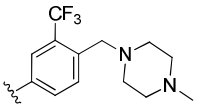	0.164±0.021	0.22±0.014	>10
13	-Me	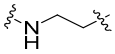	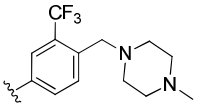	1.55±0.001	3.3±0.104	>10
14	-Me	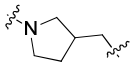	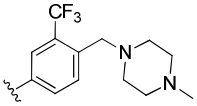	4.94±1.00	3.82±0.045	3.98±0.021
15	-Me	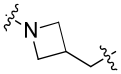	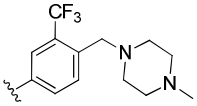	5.40±0.146	2.86±0.145	1.07±0.012
16	-Cl	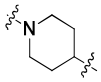	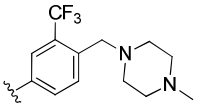	0.253±0.092	0.34±0.014	>10
17	-OMe	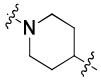	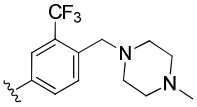	8.41±2.54	>10	>10

[a]All GI_{50} values were obtained by triplet testing.

We next explored the hinge-binding moiety (R2) (Table 2). Compared to nicotinamide (**12**), 2-(pyridin-3-yl)acetamide (**18**) lost activity to ABL and c-KIT kinase significantly. Smaller propionyl (**19**) and acryloyl group (**20**) as the head moieties largely reduced the potencies to ABL while the potencies to c-KIT were retained. Installation of *N, N*-dimethyl hydrophilic moiety on the head (**21**) lowered the potencies to micromole level both to ABL and c-KIT. Replacing the pyridine with a more hydrophobic benzene group (**22**) lost 4-fold activity against

ABL and 2-fold against c-KIT kinase. Switching the nitrogen atom from 3- position to 2-position (**23**) and 4- position (**24**) increased about 2-fold potency to ABL kinase meanwhile kept the activity against c-KIT kinase. Replacement of pyridine with thiophene (**25**) started to inhibit the parental BaF3 cell, while furan-3-carbonyl (**26)** retained similar activity trends to compound **12**. Interestingly, quinoline-3-carbonyl (**27**), 2-fluoronicotinoyl (**28**), 5-chloronicotinoyl (**29**), 2-chloronicotinoyl (**30**), 2-methylnicotinoyl (**31**), 4-methylnicotinoyl (**32**) and 5-methylnicotinoyl (**33**) all displayed toxicities against parental BaF3 cells. However, 4-methylnicotinoyl (**34**) exhibited good selectivity window between the parental BaF3 cell and ABL/c-KIT engineered isogenic cells. Furthermore, **34** increased about 5-fold potency against ABL kinase (GI_{50}: 0.033 μM) and retained the activity against c-KIT kinase (GI_{50}: 0.149 μM) compared to compound **12**. 6-Oxo-1,6-dihydropyridine-3-carbonyl (**35**) lost activities significantly to both ABL and c-KIT kinases. 2-Aminopyrimidine-5-carbonyl (**36**) presented similar activities to compound **12** against ABL kinase (GI_{50}: 0.168 μM) and c-KIT kinase (GI_{50}: 0.20 μM), meanwhile kept the selectivity window to parental BaF3 cell (GI_{50}: >10 μM). Replacement of the amide with sulfonamide (**37**) significantly lost activity to ABL kinase and started to gain toxicity to the parental BaF3 cell. Removing the amide linkage and installment of the heterocycles, *i.e.*, quinazoline (**38**) and pyrimidine (**39**) directly to the piperidine linker either exhibited toxicity to the parental BaF3 cell or significantly lost activities to ABL and c-KIT kinases.

Table 2. SAR Exploration Focused on the Hinge Binding (R2) Moiety [a]

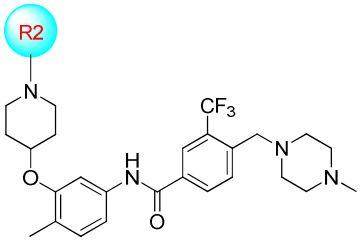

Compd	R2	P210-BaF3 (GI_{50}: μM)	Tel-c-KIT BaF3 (GI_{50}: μM)	WT- BaF3 (GI_{50}: μM)
18	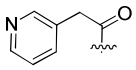	5.52±0.147	0.78±0.043	6.493±0.41
19		0.998±0.094	0.30±0.054	>10
20		0.427±0.069	0.16±0.064	>10
21	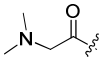	3.07±0.145	1.63±0.10	>10
22	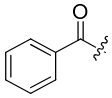	0.635±0.139	0.55±0.046	4.73±0.21
23	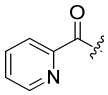	0.072±0.021	0.20±0.038	>10
24	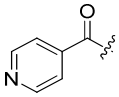	0.088±0.007	0.17±0.047	>10
25	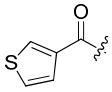	0.135±0.001	0.026±0.005	1.48±0.068
26	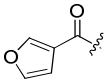	0.153±0.01	0.27±0.098	>10
27	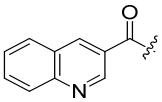	0.086±0.01	0.32±0.058	1.3±0.098
28	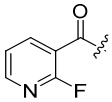	2.0±0.143	0.063±0.014	1.52±0.068
29	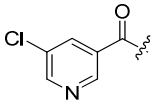	0.219±0.014	0.037±0.034	2.87±0.056

30	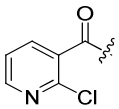	2.76±0.535	0.062±0.034	2.72±0.054
31	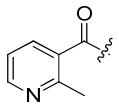	2.21±0.316	0.37±0.075	0.54±0.067
32	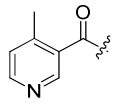	0.203±0.421	0.21±0.074	2.68±0.14
33	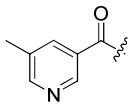	0.079±0.002	0.028±0.001	0.8±0.045
34	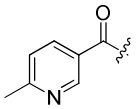	0.033±0.007	0.149±0.031	>10
35	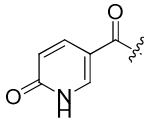	1.97±0.117	1.60±0.034	>10
36	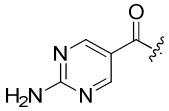	0.168±0.063	0.20±0.002	>10
37	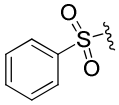	4.77±0.527	0.6±0.035	5.10±0.097
38	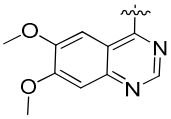	0.773±0.227	0.19±0.014	1.20±0.068
39		3.22±0.652	2.50±0.11	8.10±0.12

[a]All GI_{50} values were obtained by triplet testing.

Biochemical and Cellular Property Evaluation

Since compounds **23-24**, **32-34** exhibited inhibitory activities against ABL and/or cKIT kinase in the BaF3 isogenic cell based assays, we then further tested them with the purified ABL1 and KIT kinases using Invitrogen's Z'lyte based biochemical activity assay and employed compound **1** as control. The results showed that compounds **23** (IC_{50}: 30 nM), **24** (IC_{50}: 7 nM),

33 (IC_{50}: 6 nM) and **34** (IC_{50}: 46 nM) possessed strong inhibitory potencies to ABL1 kinase, and all of them were more potent than **1** (IC_{50}: 223 nM) (Figure 3A). Interestingly, **32** did not show apparent inhibition to ABL1 kinase (IC_{50}: 7252 nM), which was consistent with the narrow growth inhibition selectivity window observed between P210-BaF3 and parental BaF3 cells. For c-KIT kinase, these compounds all displayed sub-micromolar inhibitory activities and **34** was the most active one (IC_{50}: 75 nM). Based on these data, we finally selected **34** as the potent ABL/c-KIT dual inhibitor for further characterization.

We next examined the kinome-wide selectivity profile of compound **34** with DiscoveRx's KINOMEscan technology.[14] The results demonstrated that **34** possessed good selectivity (S score (1) = 0.03 at 1 μM) among the 468 kinases and mutants tested. Besides ABL1 and c-KIT kinases, **34** also displayed strong binding against BLK, CSF1R, DDR1/2, LCK, LOK, and PDGFRβ kinases (percent activity remaining less than 1% at 1 μM of the inhibitor) (Figure 3B and Supplemental Table 1). Given the fact that KINOMEscan is a binding assay and may not fully reflect the inhibitory activities, we then used Invitrogen's Z'lyte based biochemical activity assay to further confirm these potential targets (Figure 3B). Besides ABL1 and c-KIT kinases, **34** also presented significant inhibitory activities to BLK ($IC_{50:}$ 81 nM), CSF1R ($IC_{50:}$ 227 nM), DDR1 ($IC_{50:}$ 116 nM), DDR2 ($IC_{50:}$ 325 nM), LCK ($IC_{50:}$ 12 nM) and PDGFRβ ($IC_{50:}$ 80 nM) kinases. In order to further confirm these targets in the cellular context, we then tested **34** on these kinase dependent isogenic BaF3 cells. Interestingly, **34** only exhibited strong anti-proliferation efficacy against PDGFRβ (GI_{50}: 0.014 μM), PDGFRα (GI_{50}: 0.012μM, Invitrogen biochemical IC_{50}: 16 nM) and VEGFR2 (GI_{50}: 0.035 μM, Invitrogen biochemical IC_{50}: 30 nM) kinases dependent cell lines (Table 3). Compound **34** presented no apparent growth inhibition to Tel-DDR1-BaF3 ($GI_{50:}$ 9.77 μM) and BCR-DDR2-BaF3 ($GI_{50:}$ 6.08 μM) cell lines and moderate

inhibitions against Tel-BLK-BaF3 (GI_{50}: 0.658 μM), Tel-CSF1R-BaF3 (GI_{50}: 0.162 μM) and Tel-LCK-BaF3 (GI_{50}: 0.386 μM), which indicated that in the cellular context **34** might not be very potent to BLK, DDR1/2, CSF1R and LCK kinases. In addition, considering that BCR-ABL and c-KIT mutations are frequently observed in clinic and some of them are critical for the drug sensitivity, we also evaluated compound **34** against these mutants in the BaF3 isogenic cells (Table 3). The data demonstrated that compound **34** was more effective against most BCR-ABL mutations than compound **1** including P210/H369P-BaF3, P210/M356T-BaF3, P210/F317L-BaF3 and P210/F317I-BaF3 but not active against P210/T315I-BaF3 ($GI_{50:}$ > 10 μM). For varieties of c-KIT mutations, compound **34** showed good inhibitory activities to c-Kit/V559D, c-Kit/L576P and c-Kit/N822K but it was less potent to other mutants such as c-Kit/V559D/V654A, c-Kit/T670I/V559D, c-Kit/V654A-BaF3, Tel-c-Kit/T670I, and c-KIT/D816V, which displayed a similar trend to compound **1**.

A

Compd.	ABL1 (IC_{50} / nM)	KIT (IC_{50} / nM)
1	223±59	164±32
23	30±5	644±177
24	7±1	256±87
32	7252±1613	336±21
33	6±0.5	214±5
34	46±6	75±6

B

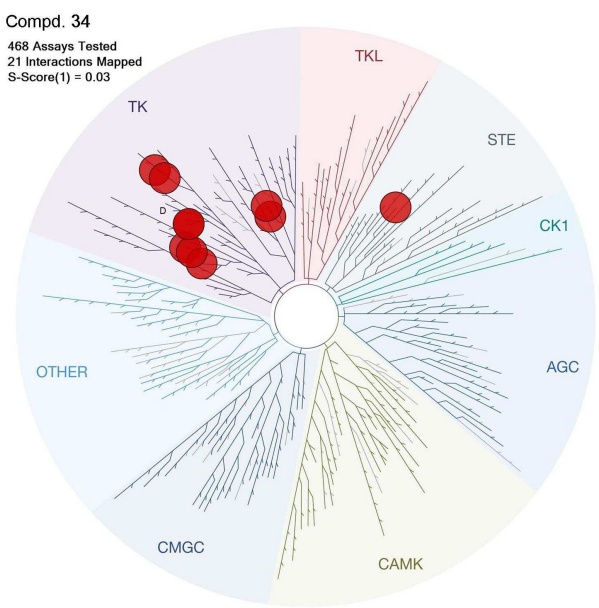

Kinase	ABL1	KIT	BLK	CSF1R	DDR1	DDR2	LCK	LOK	PDGFRβ
Percent control at 1 μM	0.3	0.8	0.45	0.3	0.35	0.65	0.55	0.6	0.3
Compd. 34 IC_{50} / nM	46 ±6	75 ±6	81 ±6	227 ±30	116 ±10	325 ±26	12 ±0.2	ND	80 ±28

Figure 3. Activity and selectivity characterization of compound **34**. (A) Biochemical assay characterization of the inhibitory activities of **1**, **23-24** and **32-34** against primary targets ABL1 and KIT kinases. (B) KINOMEscan profiling of **34** at a concentration of 1 μM against 468 kinases and its biochemical inhibitory activities to the selected kinases.

Table 3. Anti-proliferative Effects of Compounds **1** and **34** against a Panel of Isogenic BaF3 Cell Lines[a]

Cell line	Compd. **1** (GI_{50}: μM)	Compd. **34** (GI_{50}: μM)
Parental BaF3	>10	>10
Tel-BLK-BaF3	>10	0.658±0.056

Tel-DDR1-BaF3	>10	9.77±0.43
BCR-DDR2-BaF3	>10	6.08±0.043
Tel-CSF1R-BaF3	0.11±0.055	0.162±0.089
Tel-LCK-BaF3	>10	0.386±0.025
Tel-PDGFRα-BaF3	0.034±0.008	0.012±0.00017
Tel-PDGFRβ-BaF3	0.019±0.007	0.014±0.00021
Tel-VEGFR2-BaF3	>10	0.035±0.00012
P210/T315I-BaF3	>10	>10
P210/Y253H-BaF3	>10	1.67±0.067
P210/H369P-BaF3	1.79±0.177	0.98±0.046
P210/M356T-BaF3	0.625±0.253	0.27±0.064
P210/F317L-BaF3	2.16±0.039	0.67±0.031
P210/F317I-BaF3	0.85±0.253	0.49±0.021
Tel-cKit-BaF3	0.37±0.031	0.149±0.031
Tel-cKit/V559D-BaF3	0.039±0.008	0.078±0.0003
Tel-cKit/V559D/V654A-BaF3	3.0±0.089	2.87±0.012
Tel-cKit/N822K-BaF3	1.29±0.057	0.124±0.009
Tel-cKit/T670I/V559D-BaF3	>10	1.01±0.007
Tel-cKit/V654A-BaF3	2.49±0.14	1.84±0.021
Tel-cKit/L576P-BaF3	0.102±0.048	0.221±0.0012
Tel-cKit/T670I-BaF3	6.67±0.24	1.85±0.004
Tel-cKit/D816V-BaF3	>10	5.06±0.012

[a] All GI_{50} values were obtained by triple testing.

We then tested compound **34** against a panel of established cancer cell lines. Not surprisingly, it exhibited better anti-proliferation activities than compound **1** in the BCR-ABL dependent CML cancer cell lines such as K562 (GI_{50}: 0.027 μM), MEG-01 (GI_{50}: 0.02 μM), and KU812 (GI_{50}: 0.056 μM). It also potently inhibited the growth of c-KIT dependent GISTs cancer cell lines including GIST-T1 (GI_{50}: 0.023 μM), GIST-882 (GI_{50}: 0.095 μM) but not c-KIT independent GIST-48B (GI_{50}: 3.96 μM). In addition, compound **34** did not show potent inhibitory activities against FLT3-ITD dependent AML cell lines, *i.e.*, MV4-11 (GI_{50}: 8.14 μM) and MOLM-14 (GI_{50}: 8.49 μM), as well as other leukemic cell lines such as U937 (GI_{50}: 5.73 μM), HL-60 (GI_{50}: 7.34 μM), REC-1 (GI_{50}: 3.47 μM). Compound **34** did not exhibit apparent inhibitory activity against the normal Chinese hamster ovary (CHO) cells ($GI_{50} > 10$ μM) either, which indicated a good selectivity window between the cancer cells and normal cells.

Table 4. Anti-proliferative Effects of Compounds **1** and **34** against a Panel of Established Cancer Cell Lines[a]

Cell line	Compd.**1** (GI_{50}: μM)	Compd. **34** (GI_{50}: μM)
K562	0.267±0.01	0.027±0.004
MEG-01	0.074±0.008	0.02±0.007
KU812	0.163±0.012	0.056±0.0009
GIST-T1	0.008±0.0002	0.023±0.0007
GIST-882	0.014±0.0003	0.095±0.005
GIST-48B	>10	3.96±0.098
MV4-11	>10	8.14±0.017

MOLM-14	>10	8.49±0.08
U937	>10	5.73±0.037
HL-60	>10	7.34±0.14
REC-1	>10	3.47±0.12
CHO	>10	>10

[a] All GI_{50} values were obtained by triple testing.

To examine the binding mechanism of compound **34**, we docked the molecule into ABL1 and c-KIT kinases based on the reported high resolution (1.53 Å) co-crystal structure of compound **12** with ABL1 kinase (PDB ID: 5HU9)[13] (Figure 4A-B). The modeling results revealed that compound **34** adopted a typical type II binding mode (DFG out conformation) both to ABL1 and c-KIT kinase, which was represented by two canonical hydrogen bonds formed by Glu286 (ABL1)/Glu640 (c-KIT) located in the c-Helix and Asp381 (ABL1 and c-KIT) located in the DFG motif with the amide bond (NHC=O) of the inhibitor. Intriguingly, compound **34** also exhibited a distinct hinge binding that utilized an amide oxygen atom to form the hydrogen bonds with Met318 in ABL kinase and Cys673 in c-KIT kinase. This was different from the classic hinge-binding mode of compounds **1**-**7**.

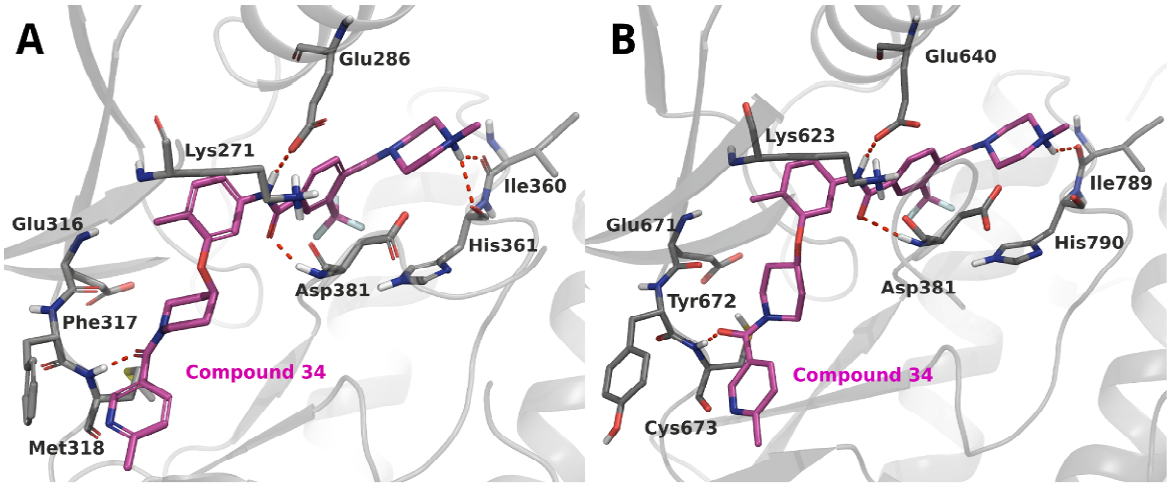

Figure 4. Binding modes of compound **34** in complex with ABL1 and c-KIT kinases. (A) Docking of **34** in complex with ABL1 kinase (PDB ID: 5HU9). (B) Docking of **34** in complex with c-KIT kinase (PDB ID: 1T46).

We then examined compound **34**'s effects on the BCR-ABL mediated signaling pathways in K562, KU812 and MEG-01 cells (Figure 5A). The results demonstrated that it potently inhibited BCR-ABL's auto-phosphorylation at Y245 site in K562 cells (EC_{50} < 100 nM) and displayed a better inhibitory activity than compound **1**. Compound **34** also significantly blocked the downstream signaling mediators such as pStat5, pCrkL and pERK in K562 cells, which also exhibited stronger potency than **1**. Similar trends were observed in the BCR-ABL dependent CML cell lines KU812 and MEG-01, which further confirmed that **34** had strong inhibitory effects on the BCR-ABL mediated signaling pathways. In other experiments, compound **34** also potently inhibited the auto-phosphorylation of c-KIT at Y703, Y719 and Y823 sites in GIST-T1 and GIST-882 cells and displayed similar inhibitory activities to compound **1** (Figure 5B). Furthermore, **34** significantly blocked downstream signaling mediators such as pAKT, pStat3/5, pERK， pS6K, pS6 in GIST-T1 and GIST-882 cells, which was similar to compound **1**. Meanwhile, **34** displayed little effect on c-KIT independent GIST-48B cells.

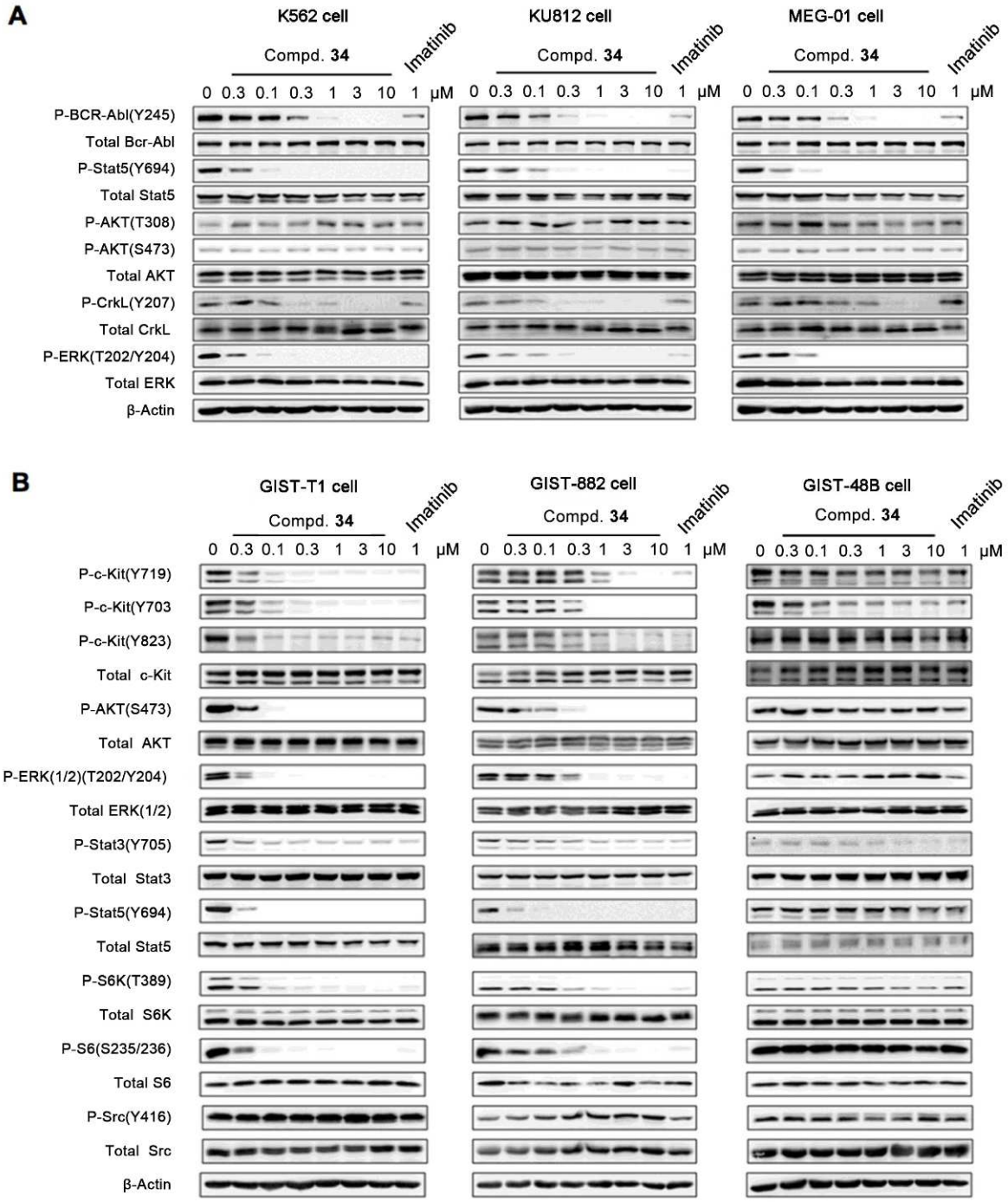

Figure 5. Effects of compounds **1** and **34** on the signaling transduction pathways. (A) Effects of **1** and **34** on the BCR-ABL mediated signaling pathways in the BCR-ABL dependent CML cell lines (K562, KU812 and MEG-01). (B) Effects of **1** and **34** on the c-KIT mediated signaling

pathways in the c-KIT dependent (GIST-T1 and GIST-882) and c-KIT independent (GIST-48B) cell lines.

In addition, compound **34** could effectively arrest the cell cycle into the G0/G1 phase starting from a concentration of 0.3 μM in K562, KU812, MEG-01 cells as well as GIST-T1 and GIST-882 cells but not GIST-48B cells (Figure 6). Similar results were observed for compound **1** at 1 μM concentration. Furthermore, apparent apoptosis was observed in K562, KU812, MEG-01, GIST-T1 and GIST-882 cells but not in GIST-48B cells by examining the cleavage of PARP and Caspase-3 proteins (Figure 7).

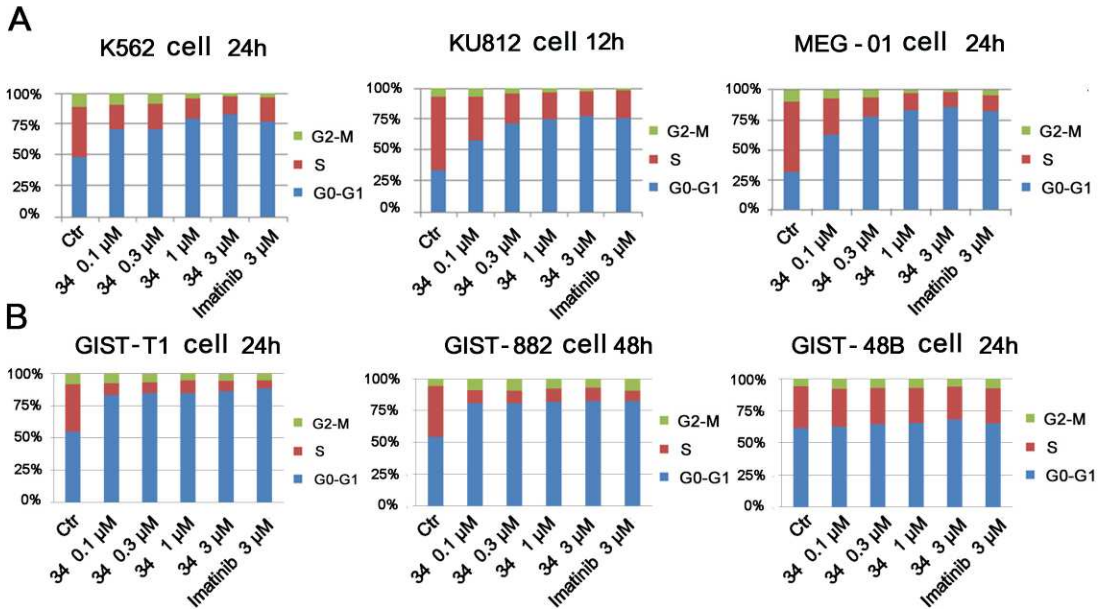

Figure 6. Effects of compounds **1** and **34** on induction of cell cycle progression in (A) K562, KU812 and MEG-01 CML cells and (B) GIST-T1, GIST-882 and GIST-48B GISTs cells.

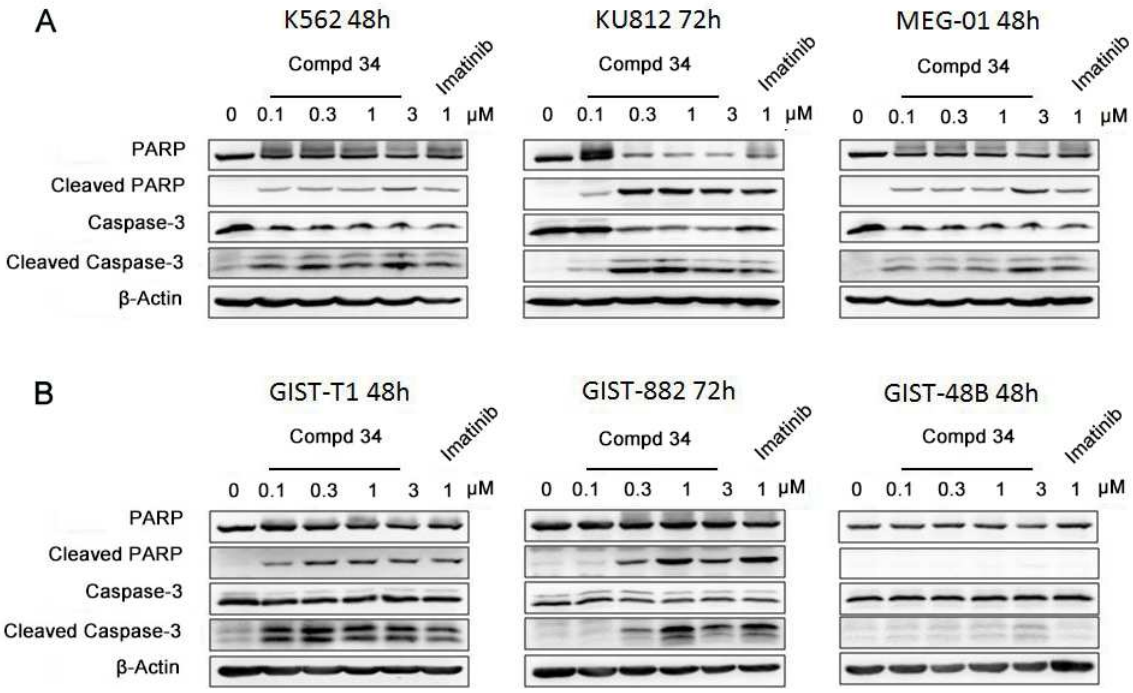

Figure 7. Effects of compounds **1** and **34** on apoptosis in (A) K562, KU812 and MEG-01 CML cells and (B) GIST-T1, GIST882 and GIST-48B GISTs cells.

In Vivo PK/PD Evaluation.

We next evaluated compound **34**'s PK properties in rats following intravenous and oral administration (Table 5). The data demonstrated that **34** possessed an acceptable bioavailability (F = 47.5%) and a suitable half-life ($T_{1/2}$ = 2.83 h) for oral administration. In the CML K562 cells inoculated xenograft mouse model, oral administration of compound **34** showed dose-dependent tumor progression suppression without apparent toxicity (Figure 8A-C). A dosage of 100 mg/kg/day exhibited TGI (tumor growth inhibition) of 66.8%, which was better than compound **1** at the same dosage (Figure 8D). Immunohistochemistry stain results demonstrated that compound **34** could dose-dependently inhibit the cancer cell proliferation (Ki-67 stain) and induce the apoptosis (TUNEL stain) (Figure 8E). Similarly, compound **34** could also dose-

dependently suppress the GIST-T1 cell mediated tumors in the xenograft mouse model with a TGI of 46.5% at a dosage of 100 mg/kg/day (Figure 9A-E).

Table 5. Pharmacokinetic Characterization of Compound **34** in Sprague Dawley Rats

Data	iv (1 mg/kg)	po (10 mg/kg)
$AUC_{0\text{-}t}$ (ng/mL*h)	510.308±55.802	2422.086±1644.633
$AUC_{0\text{-}\infty}$(ng/mL*h)	557.859±58.155	2432.354±1653.435
$MRT_{(0\text{-}t)}$(h)	1.933±0.222	5.746±1.179
C_{max}(ng/mL)	825.144±197.748	222.966±114.288
T_{max}(h)	0.017±0	6±0
$T_{1/2}$(h)	2.469±0.466	2.828±0.039
F (%)	-	47.46

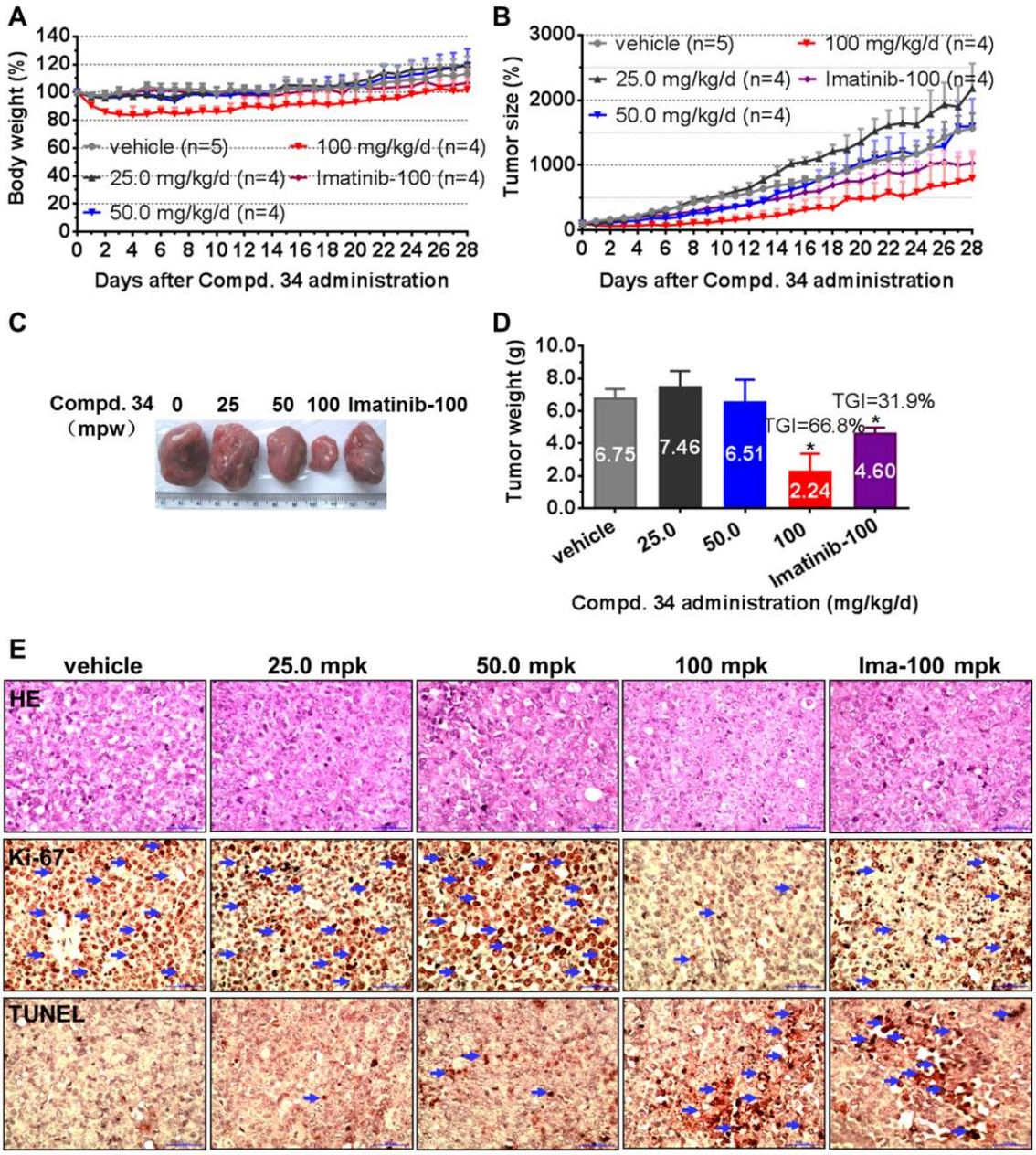

Figure 8. Compound **34**'s anti-tumor efficacy in K562 xenograft mouse model. Female nu/nu mice bearing established K562 tumor xenografts were treated with **34** at 25.0, 50.0 and 100 mg/kg/d dosage, 100 mg/kg/d imatinib or vehicle. Daily oral administration was initiated when K562 tumors had reached a size of 200 to 400 mm^3. Each group contained 4 or 5 animals. Data, mean ± SEM. (A) Body weight and (B) Tumor size measurements from K562 xenograft mice after **34** and imatinib administration. Initial body weight and tumor size were set as 100%. (C)

Representative photographs of tumors in each group after 0, 25.0, 50.0 or 100 mg/kg/d **34** and 100 mg/kg/d imatinib treatment. (D) Comparison of the final tumor weight in each group after 28-day treatment period of **34** and imatinib. Numbers in columns indicate the mean tumor weight in each group. *$p<0.05$. (E) Representative micrographs of hematoxylin and eosin (HE), Ki-67, and TUNEL staining of tumor tissues with **34** treatment groups in comparison with the vehicle and imatinib treatment group. Note the specific nuclear staining of cells with morphology consistent with proliferation and apoptosis (E, blue arrow).

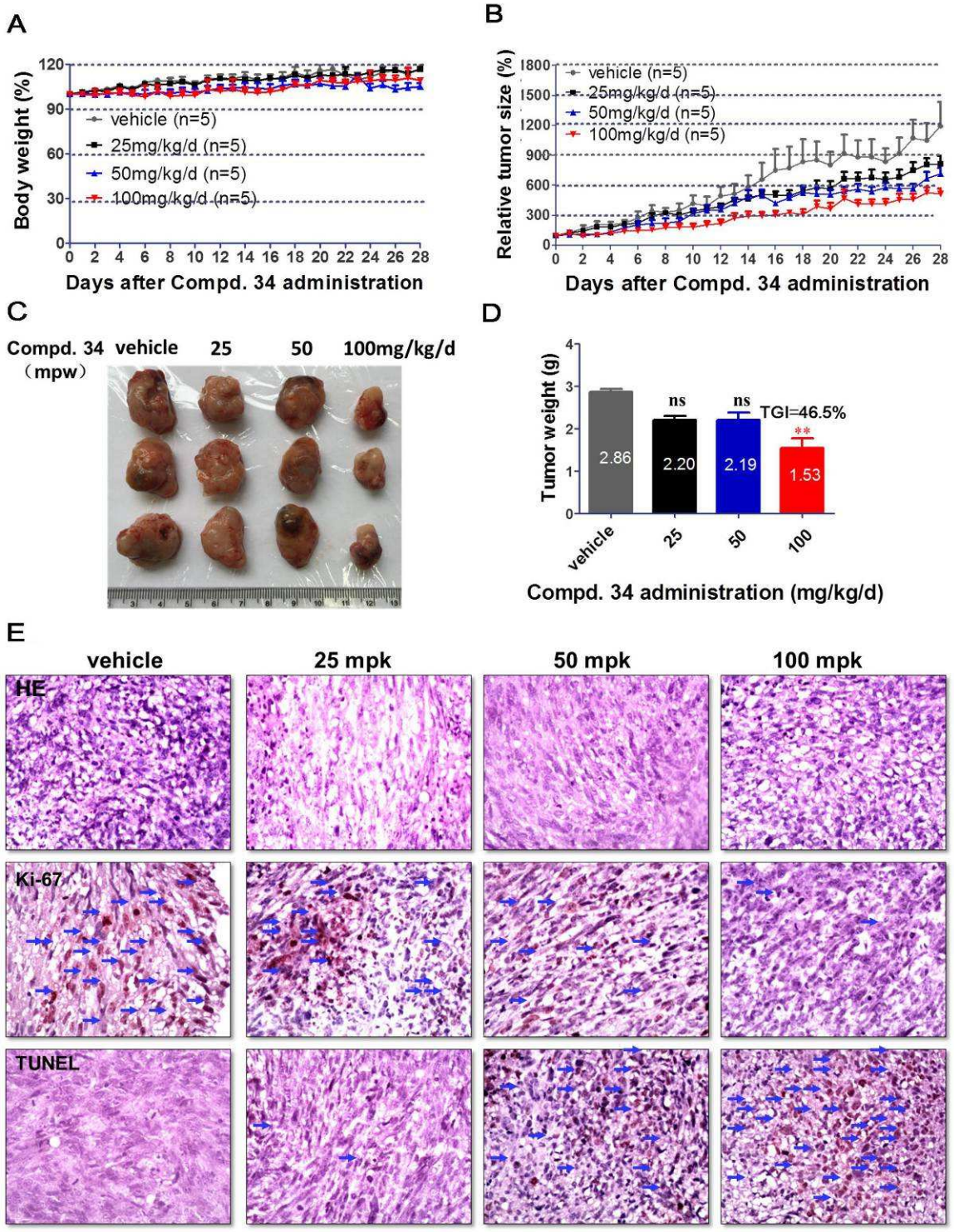

Figure 9. Compound **34**'s anti-tumor efficacy in GIST-T1 xenograft mouse model. Female nu/nu mice bearing established GIST-T1 tumor xenografts were treated with **34** at 25.0, 50.0 and

100 mg/kg/d dosage, or vehicle. Daily oral administration was initiated when GIST-T1 tumors had reached a size of 200 to 400 mm^3. Each group contained 5 animals. Data, mean ± SEM. (A) Body weight and **(**B**)** Tumor size measurements from GIST-T1 xenograft mice after **34** administration. Initial body weight and tumor size were set as 100%. (C) Representative photographs of tumors in each group after 25.0, 50.0 or 100 mg/kg/d **34** or vehicle treatment. (D) Comparison of the final tumor weight in each group after 21-day treatment period of **34**. Numbers in columns indicate the mean tumor weight in each group. ns, $p>0.05$, $*p<0.05$, $**p<0.01$. (E) Representative micrographs of hematoxylin and eosin (HE), Ki-67, and TUNEL staining of tumor tissues with **34** treatment groups in comparison with the vehicle group. Note the specific nuclear staining of cells with morphology consistent with proliferation and apoptosis (E, blue arrow).

CONCLUSIONS

Based on structure guided drug design and hybrid drug design approaches, we have discovered a type II kinase inhibitor **34** showing strong inhibitory potency to BCR-ABL, c-KIT etc kinases. Importantly, compound **34** adopted a distinct hinge binding mode that the amide oxygen served as the hinge binding hydrogen bond donor. This is different from classical hinge bindings and may bring more opportunities for new type II inhibitor discovery. In the following extensive biological characterization, **34** exhibited good activity and selectivity only with finite kinase targets. Compound **34** also potently inhibited VEGFR2, PDGFRα/β, DDR1 and CSF1-R kinases, which might contribute to its anti-tumor activity since PDGFRs and VEGFR2 play critical roles in angiogenesis.[15, 16] DDR1 kinase plays role in the tumor proliferation, migration and invasion,[17] and CSF1-R is essential for cell survival, proliferation and differentiation.[18]

However, it should be noted that these off-targets may also potentially induce the adverse events in the clinic context. It is also worthy to note that compound **34** was not active to imatinib-resistant BCR-ABL mutant T315I and c-KIT mutants such as V654A, D816V etc, which are important mutants observed in the clinic. Further detailed SAR study based on this pharmacophore is required for achievement of potency against those drug resistant mutants. Besides, the good PK profile and anti-tumor efficacy in vivo suggested that compound **34** might be a good potential drug candidate and currently it is under extensive preclinical evaluation.

EXPERIMENTAL SECTION

Chemistry. All reagents and solvents were purchased from commercial sources and used as obtained. ^{1}H NMR and ^{13}C NMR spectra were recorded with a Bruker 400 NMR spectrometer and referenced to deuterium dimethyl sulfoxide (DMSO-d_6) or deuterium chloroform ($CDCl_3$). Chemical shifts are expressed in ppm. In the NMR tabulation, s indicates singlet; d, doublet; t, triplet; q, quartet; m, multiplet; and br, broad peak. LC/MS were performed on *an* Agilent 6224 TOF using an ESI source coupled to an Agilent 1260 Infinity HPLC system operating in reverse mode with an Agilent Eclipse Plus C18 1.8 μm 3.0×50 mm column. Flash column chromatography was conducted using silica gel (Silicycle 40−64 μm). The purities of all compounds were determined to be above 95% by HPLC.

*N-(4-Methyl-3-((1-nicotinoylpiperidin-4-yl)oxy)phenyl)-4-((4-methylpiperazin-1-yl)methyl)benzamide (**11**)*. **44g** (0.05 mmol, 15.6 mg), HATU (0.06 mmol, 23 mg), and DIPEA (0.075 mmol, 10 mg) were dissolved in 0.5 mL of DMF and cooled to 0 °C. Then 4-((4-methylpiperazin-1-yl)methyl)benzoic acid (0.06 mmol, 14 mg) was added to the system and the mixture was stirred at room temperature for 2 h, then extracted with EtOAc and dried with anhydrous Na_2SO_4. The solvent was removed under vacuum and the residue was purified by

silica gel flash chromatography (DCM/MeOH = 10/1) to offer the product **12** (17.1 mg, 65 %) as a white solid. ^{1}H NMR (400 MHz, DMSO-d_6) δ 10.16 (s, 1H), 8.67 (s, 2H), 8.04 - 7.82 (m, 3H), 7.52 (s, 4H), 7.33 (d, J = 6.4 Hz, 1H), 7.13 (d, J = 5.8 Hz, 1H), 4.61 (s, 1H), 3.97 - 3.48 (m, 6H), 3.07 - 2.78 (m, 7H), 2.17 (s, 3H), 2.04 (s, 2H), 1.79 (s, 2H). LC/MS (ESI, m/z): 528.2891 $[M+H]^+$.

Compounds **12-36** were prepared following the synthetic procedure of **11**.

*N-(4-Methyl-3-((1-nicotinoylpiperidin-4-yl)oxy)phenyl)-4-((4-methylpiperazin-1-yl)methyl)-3-(trifluoromethyl)benzamide (**12**)*. Yield 69%. ^{1}H NMR (400 MHz, DMSO-d_6) δ 10.42 (s, 1H), 8.64 (s, 2H), 8.26 - 8.24 (m, 2H), 7.91 - 7.86 (m, 2H), 7.51 - 7.47 (m, 2H), 7.31 (d, J = 7.6 Hz, 1H), 7.13 (d, J = 7.6 Hz, 1H), 4.59 (m, 1H), 3.83 - 3.52 (m, 6H), 2.66 (s, 8H), 2.37 (s, 3H), 2.15 (s, 3H), 1.98 (s, 2H), 1.75 (s, 2H). LC/MS (ESI, m/z): 595.2776 $[M+H]^+$.

*N-(2-(2-Methyl-5-(4-((4-methylpiperazin-1-yl)methyl)-3-(trifluoromethyl)benzamido)phenoxy)ethyl)nicotinamide (**13**)*. Yield 81%. ^{1}H NMR (400 MHz, DMSO-d_6) δ 10.40 (s, 1H), 9.04 (s, 1H), 8.97 (s, 1H), 8.72 (s, 1H), 8.28 (s, 3H), 7.93 (s, 1H), 7.53 (s, 2H), 7.30 (s, 1H), 7.13 (s, 1H), 4.14 (s, 2H), 3.76 (s, 4H), 2.94 (s, 4H), 2.58 (s, 7H), 2.14 (s, 3H). LC/MS (ESI, m/z): 556.2461 $[M+H]^+$.

*N-(4-Methyl-3-((1-nicotinoylpyrrolidin-3-yl)methoxy)phenyl)-4-((4-methylpiperazin-1-yl)methyl)-3-(trifluoromethyl)benzamide (**14**)*. Yield 76%. ^{1}H NMR (400 MHz, DMSO-d_6) δ 10.39 (s, 1H), 8.73 (s, 1H), 8.65 (s, 1H), 8.25 (s, 2H), 7.95 - 7.91 (m, 2H), 7.45 (s, 2H), 7.36 - 7.17 (m, 1H), 7.19 - 6.88 (m, 1H), 4.09 - 3.82 (m, 2H), 3.81 - 3.36 (m, 6H), 2.87 (s, 4H), 2.74 (s, 1H), 2.67 - 2.49 (m, 7H), 2.15 - 2.04 (m, 4H), 1.84 (s, 1H). LC/MS (ESI, m/z): 596.2776 $[M+H]^+$.

*N-(4-Methyl-3-((1-nicotinoylazetidin-3-yl)methoxy)phenyl)-4-((4-methylpiperazin-1-yl)methyl)-3-(trifluoromethyl)benzamide (**15**)*. Yield 81%. ^{1}H NMR (400 MHz, DMSO-d_6) δ

10.41 (s, 1H), 9.02 – 8.69 (m, 2H), 8.26 (s, 2H), 8.02 (s, 1H), 7.91 (d, J = 7.5 Hz, 1H), 7.49 (s, 2H), 7.28 (d, J = 8.2 Hz, 1H), 7.11 (s, 1H), 4.53 (s, 1H), 4.28 - 3.82 (m, 4H), 3.74 (s, 2H), 3.35 (s, 1H), 3.12 (s, 1H), 2.90 (s, 4H), 2.56 (s, 7H), 2.08 (s, 3H). LC/MS (ESI, m/z): 582.2606 $[M+H]^+$.

*N-(4-Chloro-3-((1-nicotinoylpiperidin-4-yl)oxy)phenyl)-4-((4-methylpiperazin-1-yl)methyl)-3-(trifluoromethyl)benzamide (**16**).* Yield 72%. ^{1}H NMR (400 MHz, DMSO-d_6) δ 10.61 (s, 1H), 8.67 (s, 2H), 8.29 (s, 2H), 7.93 (m, 2H), 7.75 (s, 1H), 7.48 (m, 3H), 4.71 (s, 1H), 3.81 - 3.33 (m, 6H), 3.04 - 2.50(m, 11H), 2.03 (s, 2H), 1.82 (s, 2H). LC/MS (ESI, m/z): 616.2219 $[M+H]^+$.

*N-(4-Methoxy-3-((1-nicotinoylpiperidin-4-yl)oxy)phenyl)-4-((4-methylpiperazin-1-yl)methyl)-3-(trifluoromethyl)benzamide (**17**).* Yield 76%. ^{1}H NMR (400 MHz, DMSO-d_6) δ 10.32 (s, 1H), 9.71 (s, 1H), 8.65 (s, 2H), 8.27 (s, 2H), 7.89 (s, 2H), 7.51 (s, 2H), 7.37 (s, 1H), 7.02 (s, 1H), 4.52 (s, 1H), 3.96 - 2.71 (m, 20H), 2.02 (s, 2H), 1.73 (s, 2H). LC/MS (ESI, m/z): 612.2712 $[M+H]^+$.

*N-(4-Methyl-3-((1-(2-(pyridin-3-yl)acetyl)piperidin-4-yl)oxy)phenyl)-4-((4-methylpiperazin-1-yl)methyl)-3-(trifluoromethyl)benzamide (**18**).* Yield 66%. ^{1}H NMR (400 MHz, DMSO-d_6) δ 10.36 (s, 1H), 8.44 (s, 2H), 8.25 (s, 2H), 7.91 (d, J = 8.0 Hz, 1H), 7.64 (d, J = 7.6 Hz, 1H), 7.47 (s, 1H), 7.34 (s, 1H), 7.27 (d, J = 8.1 Hz, 1H), 7.13 (d, J = 8.1 Hz, 1H), 4.54 (s, 1H), 3.80 - 3.77 (m, 6H), 3.45 (s, 2H), 3.09 (s, 4H), 2.69 (s, 7H), 2.14 (s, 3H), 1.94 (s, 2H), 1.67 (s, 2H). LC/MS (ESI, m/z): 610.2933 $[M+H]^+$.

*N-(4-Methyl-3-((1-propionylpiperidin-4-yl)oxy)phenyl)-4-((4-methylpiperazin-1-yl)methyl)-3-(trifluoromethyl)benzamide (**19**).* Yield 76%. ^{1}H NMR (400 MHz, DMSO-d_6) δ 10.37 (s, 1H), 8.23 (s, 2H), 7.91 (d, J = 8.1 Hz, 1H), 7.48 (s, 1H), 7.28 (d, J = 7.9 Hz, 1H), 7.12 (d, J = 7.9 Hz, 1H), 4.54 (s, 1H), 3.69 (s, 4H), 3.64 (s, 2H), 2.49 - 2.17 (m, 13H), 2.14 (s, 3H), 1.93 (s, 2H), 1.66 (s, 2H), 1.06 - 0.92 (m, 3H). LC/MS (ESI, m/z): 547.2830 $[M+H]^+$.

N-(3-((1-Acryloylpiperidin-4-yl)oxy)-4-methylphenyl)-4-((4-methylpiperazin-1-yl)methyl)-3-(trifluoromethyl)benzamide ***(20)***. Yield 82%. ^{1}H NMR (400 MHz, DMSO-d_6) δ 10.35 (s, 1H), 8.23 (s, 1H), 8.21 (s, 1H), 7.92 (d, J = 7.2Hz, 1H), 7.74 (s, 1H), 7.29 (d, J = 8.0Hz, 1H), 7.13 (d, J = 8.0Hz, 1H), 6.84 (m, 1H), 6.13 (d, J = 6.4Hz, 1H), 5.69 (d, J = 10.4Hz,1H),4.56 (m, 1H), 3.75 - 3.53 (m, 6H), 2.44 (s, 8H), 2.23 (s, 3H), 2.14 (s, 3H), 1.95 (s, 2H), 1.68 (s, 2H). LC/MS (ESI, m/z): 545.2666 $[M+H]^+$.

N-(3-((1-(2-(Dimethylamino)acetyl)piperidin-4-yl)oxy)-4-methylphenyl)-4-((4-methylpiperazin-1-yl)methyl)-3-(trifluoromethyl)benzamide ***(21)***. Yield 81%. ^{1}H NMR (400 MHz, DMSO-d_6) δ 10.41 (s, 1H), 8.27 (s, 2H), 7.93 (s, 1H), 7.54 (s, 1H), 7.26 (d, J = 6.4 Hz, 2H), 7.14 (d, J = 8.4 Hz, 1H), 4.60 (s, 1H), 4.24 (s, 2H), 3.77 (s, 4H), 3.53 (s, 2H), 3.13 -.251 (m, 17H), 2.12(s, 3H), 2.01 (s, 2H), 1.79 (s, 2H). LC/MS (ESI, m/z): 576.3091 $[M+H]^+$.

N-(3-((1-Benzoylpiperidin-4-yl)oxy)-4-methylphenyl)-4-((4-methylpiperazin-1-yl)methyl)-3-(trifluoromethyl)benzamide ***(22)***. Yield 75%. ^{1}H NMR (400 MHz, DMSO-d_6) δ 10.38 (s, 1H), 8.24 (s, 2H), 7.90 (s, 1H), 7.46 (m, 6H), 7.28 (s, 1H), 7.13 (d, J = 7.4 Hz, 1H), 4.58 (s, 1H), 3.82 - 3.52(m, 6H), 2.69 - 2.41 (s, 8H), 2.41 (s, 3H), 2.16 (s, 3H), 1.99 (s, 2H), 1.72 (s, 2H). LC/MS (ESI, m/z): 595.2826 $[M+H]^+$.

N-(4-Methyl-3-((1-picolinoylpiperidin-4-yl)oxy)phenyl)-4-((4-methylpiperazin-1-yl)methyl)-3-(trifluoromethyl)benzamide ***(23)***. Yield 79%. ^{1}H NMR (400 MHz, DMSO-d_6) δ 10.40 (s, 1H), 8.59 (d, J = 4.2 Hz, 1H), 8.27 (s, 2H), 7.93 (t, J = 7.6 Hz, 2H), 7.58 (d, J = 7.6 Hz, 1H), 7.52 - 7.41 (m, 2H), 7.29 (d, J = 8.1 Hz, 1H), 7.13 (d, J = 8.1 Hz, 1H), 4.61 (s, 1H), 3.86 - 3.57 (m, 6H), 3.05 (s, 4H), 2.64 (s, 7H) 2.16 (s, 3H), 2.01 (s, 2H), 1.75 (s, 2H). LC/MS (ESI, m/z): 596.2782 $[M+H]^+$.

*N-(3-((1-Isonicotinoylpiperidin-4-yl)oxy)-4-methylphenyl)-4-((4-methylpiperazin-1-yl)methyl)-3-(trifluoromethyl)benzamide (**24**).* Yield 76%. ^{1}H NMR (400 MHz, DMSO-d_6) δ 10.41 (s, 1H), 8.67 (d, J = 5.0 Hz, 2H), 8.26 (s, 2H), 7.91 (d, J = 8.6 Hz, 1H), 7.50 (s, 1H), 7.43 (d, J = 4.8 Hz, 2H), 7.29 (d, J = 8.3 Hz, 1H), 7.13 (d, J = 7.8 Hz, 1H), 4.59 (s, 1H), 3.93 - 3.31 (m, 6H), 3.00 (s, 4H), 2.62 - 2.52 (m, 7H), 2.16 (s, 3H), 2.00 (s, 2H), 1.77 (s, 2H). LC/MS (ESI, m/z): 596.2781[M+H]$^+$.

*N-(4-Methyl-3-((1-(thiophene-3-carbonyl)piperidin-4-yl)oxy)phenyl)-4-((4-methylpiperazin-1-yl)methyl)-3-(trifluoromethyl)benzamide (**25**).* Yield 86%. ^{1}H NMR (400 MHz, DMSO-d_6) δ 10.40 (s, 1H), 8.26 (s, 2H), 7.91 (d, J = 7.8 Hz, 1H), 7.81 (s, 1H), 7.62 (s, 1H), 7.49 (s, 1H), 7.36 - 7.01 (m, 3H), 4.59 (s, 1H), 3.5 - 3.10 (m, 6H), 2.94 (s, 4H), 2.59 (m, 7H), 2.16 (s, 3H), 1.99 (s, 2H), 1.74 (s, 2H). LC/MS (ESI, m/z): 601.2377 [M+H]$^+$.

*N-(3-((1-(Furan-2-carbonyl)piperidin-4-yl)oxy)-4-methylphenyl)-4-((4-methylpiperazin-1-yl)methyl)-3-(trifluoromethyl)benzamide (**26**).* Yield 76%. ^{1}H NMR (400 MHz, DMSO-d_6) δ 10.39 (s, 1H), 8.25 (s, 2H), 7.91 (d, J = 7.8 Hz, 1H), 7.84 (s, 1H), 7.50 (s, 1H), 7.29 (d, J = 8.0 Hz, 1H), 7.13 (d, J = 8.0 Hz, 1H), 7.00 (d, J = 3.3 Hz, 1H), 6.63 (s, 1H), 4.61 (s, 1H), 3.86 - 3.67 (m, 6H), 2.77 - 2.55 (m, 8H), 2.45 (s, 3H), 2.15 (s, 3H), 2.02 (s, 2H), 1.76 (s, 2H). LC/MS (ESI, m/z): 585.2618 [M+H]$^+$.

*N-(4-Methyl-3-((1-(quinoline-3-carbonyl)piperidin-4-yl)oxy)phenyl)-4-((4-methylpiperazin-1-yl)methyl)-3-(trifluoromethyl)benzamide (**27**).* Yield 69%. ^{1}H NMR (400 MHz, DMSO-d_6) δ 10.39 (s, 1H), 8.95 (s, 1H), 8.51 (s, 1H), 8.24 (d, J = 6.4 Hz, 2H), 8.21 - 7.98 (m, 2H), 8.00 - 7.72 (m, 2H), 7.69 (t, J = 7.6 Hz, 1H), 7.51 (s, 1H), 7.29 (d, J = 8.0 Hz, 1H), 7.13 (d, J = 8.2 Hz, 1H), 4.63 (s, 1H), 3.90 - 2.55 (m, 6H), 2.89 (s, 4H), 2.59 - 2.46 (s, 7H), 2.17 (s, 3H), 2.06 (s, 2H), 1.82 (s, 2H). LC/MS (ESI, m/z): 646.2920 [M+H]$^+$.

N-(3-((1-(2-Fluoronicotinoyl)piperidin-4-yl)oxy)-4-methylphenyl)-4-((4-methylpiperazin-1-yl)methyl)-3-(trifluoromethyl)benzamide ***(28)***. Yield 81%. ^{1}H NMR (400 MHz, DMSO-d_6) δ 10.39 (s, 1H), 8.34 (s, 1H), 8.26 (s, 2H), 8.08 (s, 1H), 7.90 (s, 1H), 7.49 (s, 2H), 7.28 (s, 1H), 7.13 (d, J = 7.3 Hz, 1H), 4.60 (s, 1H), 3.83 - 2.57 (m, 17H), 2.16 (s, 3H), 2.02 (s, 2H), 1.72 (s, 2H). LC/MS (ESI, m/z): 614.2683 $[M+H]^+$.

N-(3-((1-(5-Chloronicotinoyl)piperidin-4-yl)oxy)-4-methylphenyl)-4-((4-methylpiperazin-1-yl)methyl)-3-(trifluoromethyl)benzamide ***(29)***. Yield 72%. ^{1}H NMR (400 MHz, DMSO-d_6) δ 10.38 (s, 1H), 8.72 (s, 1H), 8.61 (s, 1H), 8.25 (s, 2H), 8.08 (s, 1H), 7.92 (s, 1H), 7.49 (s, 1H), 7.28 (s, 1H), 7.14 (s, 1H), 4.60 (s, 1H), 3.73-2.52 (m, 17H), 2.16 (s, 3H), 2.01 (s, 2H), 1.83 (s, 2H). LC/MS (ESI, m/z): 630.2389 $[M+H]^+$.

N-(3-((1-(2-Chloronicotinoyl)piperidin-4-yl)oxy)-4-methylphenyl)-4-((4-methylpiperazin-1-yl)methyl)-3-(trifluoromethyl)benzamide ***(30)***. Yield 66%. ^{1}H NMR (400 MHz, DMSO-d_6) δ 10.38 (s, 1H), 8.48 (s, 1H), 8.24 (s, 2H), 8.01 - 7.77 (m, 2H), 7.52 - 7.49 (m, 2H), 7.27 (s, 1H), 7.13 (d, J = 5.7 Hz, 1H), 4.59 (s, 1H), 3.84 - 2.51 (m, 17H), 2.15 (s, 3H), 1.94 (s, 2H), 1.73 (s, 2H). LC/MS (ESI, m/z): 630.2376 $[M+H]^+$.

N-(4-Methyl-3-((1-(2-methylnicotinoyl)piperidin-4-yl)oxy)phenyl)-4-((4-methylpiperazin-1-yl)methyl)-3-(trifluoromethyl)benzamide ***(31)***. Yield 61%. ^{1}H NMR (400 MHz, DMSO-d_6) δ 10.40 (s, 1H), 8.50 (s, 1H), 8.26 (s, 2H), 7.90 (s, 1H), 7.67 (s, 1H), 7.49 (s, 1H), 7.27 (s, 2H), 7.13 (d, J = 7.8 Hz, 1H), 4.58 (s, 1H), 3.90 - 3.05 (m, 6H), 2.67 (s, 8H), 2.42 (s, 3H), 2.26 - 1.46 (m, 7H). LC/MS (ESI, m/z): 610.2936 $[M+H]^+$.

N-(4-Methyl-3-((1-(4-methylnicotinoyl)piperidin-4-yl)oxy)phenyl)-4-((4-methylpiperazin-1-yl)methyl)-3-(trifluoromethyl)benzamide ***(32)***. Yield 66%. ^{1}H NMR (400 MHz, DMSO-d_6) δ 10.38 (s, 1H), 8.47 (s, 1H), 8.42 (s, 1H), 8.24 (d, J = 9.4 Hz, 2H), 7.91 (d, J = 8.3 Hz, 1H), 7.48

(s, 1H), 7.38 - 7.21 (m, 2H), 7.13 (d, J = 6.8 Hz, 1H), 4.58 (s, 1H), 3.79 - 3.19 (m, 6H), 2.97 (m, 11H), 2.15 (s, 3H), 2.02 (s, 3H), 1.97 - 1.78 (m, 4H). LC/MS (ESI, m/z): 610.2936 $[M+H]^+$.

N-(4-Methyl-3-((1-(5-methylnicotinoyl)piperidin-4-yl)oxy)phenyl)-4-((4-methylpiperazin-1-yl)methyl)-3-(trifluoromethyl)benzamide ***(33)*****.** Yield 76%. ^{1}H NMR (400 MHz, DMSO-d_6) δ 10.40 (s, 1H), 8.49 (s, 1H), 8.44 (s, 1H), 8.25 (d, J = 6.6 Hz, 2H), 7.91 (d, J = 7.7 Hz, 1H), 7.69 (s, 1H), 7.49 (s, 1H), 7.29 (d, J = 8.0 Hz, 1H), 7.13 (d, J = 8.2 Hz, 1H), 4.59 (s, 1H), 3.81 - 3.31 (m, 6H), 3.07 - 2.57 (m, 11H), 2.34 (s, 3H), 2.16 (s, 3H), 2.02 (s, 2H), 1.75 (s, 2H). LC/MS (ESI, m/z): 610.2921 $[M+H]^+$.

N-(4-Methyl-3-((1-(6-methylnicotinoyl)piperidin-4-yl)oxy)phenyl)-4-((4-methylpiperazin-1-yl)methyl)-3-(trifluoromethyl)benzamide ***(34)****.* Yield 72%. ^{1}H NMR (400 MHz, DMSO-d_6) δ 10.38 (s, 1H), 8.51 (s, 1H), 8.25 (s, 2H), 7.91 (d, J = 6.6 Hz, 1H), 7.76 (d, J = 6.7 Hz, 1H), 7.49 (s, 1H), 7.31 (d, 7.8 Hz, 2H), 7.13 (d, J = 7.3 Hz, 1H), 4.59 (s, 1H), 3.67 (m, 6H), 2.94 - 2.59 (s, 14H), 2.16 (s, 3H), 2.02 (s, 2H), 1.76 (s, 2H). LC/MS (ESI, m/z): 610.2936 $[M+H]^+$.

N-(4-Methyl-3-((1-(6-oxo-1,6-dihydropyridine-3-carbonyl)piperidin-4-yl)oxy)phenyl)-4-((4-methylpiperazin-1-yl)methyl)-3-(trifluoromethyl)benzamide ***(35)****.* Yield 78%. ^{1}H NMR (400 MHz, DMSO-d_6) δ 11.94 (s, 1H), 10.46 (s, 1H), 8.31 (s, 2H), 7.96 (s, 1H), 7.59 (m, 3H), 7.33 (s, 1H), 7.17 (s, 1H), 6.39 (s, 1H), 4.62 (s, 1H), 3.78 - 3.34 (m, 6H), 2.97 - 2.50 (m, 11H), 2.19 (s, 3H), 2.02 (s, 2H), 1.77 (s, 2H). LC/MS (ESI, m/z): 612.2736 $[M+H]^+$.

N-(3-((1-(2-Aminopyrimidine-5-carbonyl)piperidin-4-yl)oxy)-4-methylphenyl)-4-((4-methylpiperazin-1-yl)methyl)-3-(trifluoromethyl)benzamide ***(36)****.* Yield 79%. ^{1}H NMR (400 MHz, DMSO-d_6) δ 10.41 (s, 1H), 8.35 (s, 2H), 8.26 (s, 2H), 7.91 (d, J = 8.4 Hz, 1H), 7.50 (s, 1H), 7.30 (d, J = 8.0 Hz, 1H), 7.13 - 7.10 (m, 3H), 4.59 (s, 1H), 3.74 - 3.54 (m, 6H), 2.89 - 2.54 (s, 11H), 2.15 (s, 3H), 1.95 (s, 2H), 1.76 (s, 2H). LC/MS (ESI, m/z): 612.2826 $[M+H]^+$.

N-(4-Methyl-3-((1-(phenylsulfonyl)piperidin-4-yl)oxy)phenyl)-4-((4-methylpiperazin-1-yl)methyl)-3-(trifluoromethyl)benzamide (37). **44a** (0.05 mmol, 15.6 mg) and DIPEA (0.075 mmol, 10 mg) were dissolved in 0.5 mL of DMF, then benzenesulfonyl chloride (0.06 mmol, 10.6 mg) was added to the system. The mixture was stirred at room temperature for 2 h, and then extracted with EtOAc and dried with anhydrous Na_2SO_4. The solvent was removed under vacuum and the residue was purified by silica gel flash chromatography (DCM/MeOH = 10/1) to offer the product **37** (18.9 mg, 60 %) as a white solid. ^{1}H NMR (400 MHz, DMSO-d_6) δ 8.24 (s, 2H), 7.90 (d, J = 8.5 Hz, 1H), 7.72 (m, 5H), 7.39 (s, 1H), 7.23 (d, J = 7.8 Hz, 1H), 7.04 (d, J = 8.1 Hz, 1H), 4.43 (s, 1H), 3.76 (s, 2H), 3.21 - 2.67 (s, 15H), 1.97 (s, 2H), 1.81 (s, 5H). LC/MS (ESI, m/z): 631.2496 $[M+H]^+$.

N-(3-((1-(6,7-Dimethoxyquinazolin-4-yl)piperidin-4-yl)oxy)-4-methylphenyl)-4-((4-methylpiperazin-1-yl)methyl)-3-(trifluoromethyl)benzamide (38). **44a** (0.05 mmol, 15.6 mg), 4-chloro-6,7-dimethoxyquinazoline (0.06 mmol, 13.4 mg) and DIPEA (0.075 mmol, 10 mg) were dissolved in 0.5 mL of n-butyl alcohol. The system was refluxed overnight, then extracted with EtOAc and dried with anhydrous Na_2SO_4. The solvent was removed under vacuum and the residue was purified by silica gel flash chromatography (DCM/MeOH = 10/1) to offer the product **38** (25.8 mg, 76 %) as a white solid. ^{1}H NMR (400 MHz, DMSO-d_6) δ 10.36 (s, 1H), 8.55 (s, 1H), 8.24 (s, 2H), 7.92 (d, J = 7.5 Hz, 1H), 7.52 (s, 1H), 7.21 - 7.12 (m, 4H), 4.65 (s, 1H), 3.93 - 3.62 (m, 12H), 2.79 - 2.26 (s, 11H), 2.18 (s, 5H), 1.95 (s, 2H). LC/MS (ESI, m/z): 679.3146 $[M+H]^+$.

Compound **39** were prepared following the synthetic procedure of **38**.

N-(4-Methyl-3-((1-(pyrimidin-2-yl)piperidin-4-yl)oxy)phenyl)-4-((4-methylpiperazin-1-yl)methyl)-3-(trifluoromethyl)benzamide (39) Yield 84%. ^{1}H NMR (400 MHz, DMSO-d_6) δ

10.37 (s, 1H), 8.37 (d, J = 4.4 Hz, 2H), 8.24 (s, 2H), 7.92 (d, J = 7.5 Hz, 1H), 7.49 (s, 1H), 7.30 (d, J = 8.1 Hz, 1H), 7.13 (d, J = 7.6 Hz, 1H), 6.62 (s, 1H), 4.59 (s, 1H), 4.05 (s, 2H), 3.71 (s, 4H), 2.54 - 2.48 (m, 7H), 2.35 (s, 3H), 2.14 (s, 3H), 1.98 (s, 2H), 1.69 (s, 2H). LC/MS (ESI, m/z): 569.2783 $[M+H]^+$.

*tert-Butyl 4-(5-amino-2-methylphenoxy) piperidine-1-carboxylate (**42a**).* **40a** (5 mmol, 0.77 g) and *tert*-butyl 4-((methylsulfonyl)oxy) piperidine-1-carboxylate (10 mmol, 2.79 g) was dissolved in 15 mL DMF, then K_2CO_3 (10 mmol, 1.38 g) was added to the system and heated at 90 °C overnight. The reaction mixture was extracted with EtOAc and dried with anhydrous Na_2SO_4. The solvent was removed under vacuum and the residue was purified by silica gel flash column chromatography (petroleum ether:EtOAc = 6:1) to give intermediate **41a** as a yellow solid. LC/MS (ESI, m/z): 359.1693 $[M+Na]^+$. Then **41a** was directly dissolved in 20 mL EtOAc and Pd/C (5%) was added. The mixture was stirred under hydrogen balloon at room temperature for 6 h. The system was filtered through diatomaceous earth and the filtrate was concentrated under vacuum. The residue was purified by silica gel flash chromatography (petroleum ether:EtOAc = 8:1) to give the desired product **42a** (1.12 g, two-step yield: 73%) as a yellow oil. ^{1}H NMR (400 MHz, DMSO-d_6) δ 6.74 (d, J = 6.0 Hz, 1H), 6.23 (s, 1H), 6.07 (d, J = 6.0 Hz, 1H), 4.78 (s, 2H), 4.37 - 4.35 (m, 1H), 3.55 (m, 2H), 3.26 (m, 2H), 1.97 (s, 3H), 1.83 (s, 2H), 1.55 (s, 2H), 1.40 (s, 9H). LC/MS (ESI, m/z): 329.1949 $[M+Na]^+$.

Compounds **42b-f** were prepared following the synthetic procedure of **42a**.

*tert-Butyl 3-((5-amino-2-methylphenoxy)methyl)pyrrolidine-1-carboxylate (**42b**).* Yield (two-step) 61%. ^{1}H NMR (400 MHz, $CDCl_3$) δ 6.88 (s, 1H), 6.21 - 6.19 (m, 2H), 3.85 (s, 2H), 3.56 - 3.21 (m, 4H), 2.69 - 2.65 (m, 1H), 2.08 (s, 4H), 1.81 (m, 1H), 1.46 (s, 9H). LC/MS (ESI, m/z): 329.1952 $[M+Na]^+$.

*tert-Butyl 3-((5-amino-2-methylphenoxy)methyl)azetidine-1-carboxylate (**42c**).* Yield (two-step) 56%. ^{1}H NMR (400 MHz, $CDCl_3$) δ 6.90 (s, 1H), 6.24 - 6.22 (m, 2H), 4.33 - 3.56 (m, 8H), 3.02 - 2.96 (m, 1H), 2.08 (s, 3H), 1.44 (s, 9H). LC/MS (ESI, m/z): 315.1793 $[M+Na]^+$.

*tert-Butyl (2-(5-amino-2-methylphenoxy)ethyl)carbamate (**42d**).* Yield (two-step) 59%. ^{1}H NMR (400 MHz, DMSO-d_6) δ 6.95 (s, 1H), 6.74 (d, J = 7.7 Hz, 1H), 6.17 (s, 1H), 6.07 (d, J = 7.6 Hz, 1H), 4.82 (s, 2H), 3.82 (s, 2H), 3.30 (d, J = 5.5 Hz, 2H), 1.98 (s, 3H), 1.40 (s, 9H). LC/MS (ESI, m/z): 267.1626 $[M+H]^+$.

*tert-Butyl 4-(5-amino-2-chlorophenoxy)piperidine-1-carboxylate (**42e**).* Yield (two-step) 71%. ^{1}H NMR (400 MHz, $CDCl_3$) δ 7.09 (d, J = 7.6 Hz，1H), 6.29-6.23 (m, 2H), 4.32 - 4.28 (m, 1H), 3.64 - 3.62 (m, 2H), 3.46 - 3.42 (m, 2H), 1.82 (s, 4H), 1.45 (s, 9H). LC/MS (ESI, m/z): 349.1403 $[M+ Na]^+$.

*tert-Butyl 4-(5-amino-2-methoxyphenoxy)piperidine-1-carboxylate (**42f**).* Yield (two-step) 69%. ^{1}H NMR (400 MHz, DMSO-d_6) δ 6.67 (d，J = 7.6 Hz，1H), 6.30 (s, 1H), 6.13 (d，J = 7.6 Hz，1H), 4.61 (s, 2H), 4.32 - 4.28 (m, 1H), 3.63 - 3.60 (m, 5H), 3.16 (s, 2H), 1.97 (s, 3H), 1.81 (s, 2H), 1.51 (s, 2H), 1.40 (s, 9H). LC/MS (ESI, m/z): 345.1898 $[M+Na]^+$.

*4-(2-Methyl-5-nitrophenoxy)piperidine hydrochloride (**42g**).* Compound **41a** (5 mmol, 1.68 g) was added into 4 N HCl in EtOAc (20 mL), and the system was stirred at room temperature for 6 h. The solid was collected and dried to give the product **42g** as a yellow solid (1.22 g, 90%). ^{1}H NMR (400 MHz, DMSO-d_6) δ 9.35 (s, 2H), 7.91 - 7.65 (m, 2H), 7.47 (d, J = 8.1 Hz, 1H), 4.92 (s, 1H), 3.16 (s, 4H), 2.29 (s, 3H), 2.17 (s, 2H), 1.95 (s, 2H). LC/MS (ESI, m/z): 237.1159 $[M+H]^+$.

*N-(4-Methyl-3-(piperidin-4-yloxy)phenyl)-4-((4-methylpiperazin-1-yl)methyl)-3-(trifluoromethyl)benzamide trihydrochloride (**44a**).* To a solution of 4-((4-methylpiperazin-1-yl)methyl)-3- (trifluoromethyl) benzoic acid (3 mmol, 906 mg) and **42a** (3 mmol, 918 mg) in 15

mL DMF was added HATU (3.6 mmol, 1.37 g) and DIPEA (4.5 mmol, 585 mg). The mixture was stirred at room temperature for 2 h and the system was quenched with water, extracted with EtOAc and dried with anhydrous Na_2SO_4. The solvents were removed under vacuum to provide the crude product **43a**. LC/MS (ESI, m/z): 491.2565 $[M+H]^+$. Then **43a** was directly dissolved in 4 N HCl in EtOAc (10 mL) and the mixture was stirred at room temperature overnight. The solid was collected and dried to give the product **44a** (915 mg, two-step yield 51%) as a white solid. ^{1}H NMR (400 MHz, DMSO-d_6) δ 10.96 (s, 1H), 10.52 (s, 1H), 9.06 (s, 1H), 9.00 (s, 1H), 8.37 - 8.23 (m, 2H), 8.02 (s, 1H), 7.55 (s, 1H), 7.30 (d, J = 7.2 Hz, 1H), 7.15 (d, J = 6.3 Hz, 1H), 4.57 (s, 1H), 3.41 - 2.76 (m, 12H), 2.16 - 1.92 (m, 10H). LC/MS (ESI, m/z): 491.2565 $[M+H]^+$.

Compounds **44b-f** were prepared following the synthetic procedure of **44a**.

*N-(4-Methyl-3-(pyrrolidin-3-ylmethoxy)phenyl)-4-((4-methylpiperazin-1-yl)methyl)-3-(trifluoromethyl)benzamide trihydrochloride (**44b**).* Yield (two-step) 56%. ^{1}H NMR (400 MHz, DMSO-d_6) δ 11.58 (s, 1H), 10.57 (s, 1H), 9.55 (s, 2H), 8.36- 8.19 (m, 3H), 7.51 (s, 1H), 7.31 (s, 1H), 7.11 (d, J = 5.2 Hz, 1H), 4.15 (s, 2H), 3.99 (s, 2H), 3.49-2.67 (m, 16H), 2.13 (s, 4H), 1.79 (s, 1H). LC/MS (ESI, m/z) : 491.2569 $[M+H]^+$.

*N-(3-(Azetidin-3-ylmethoxy)-4-methylphenyl)-4-((4-methylpiperazin-1-yl)methyl)-3-(trifluoromethyl)benzamide trihydrochloride (**44c**).* Yield (two-step) 67%. ^{1}H NMR (400 MHz, DMSO-d_6) δ 11.96 (s, 1H), 10.68 (s, 1H), 9.62 (s, 2H), 8.57 (s, 1H), 8.42 (s, 1H), 8.36 (s, 2H), 7.55 (s, 1H), 7.37 (s, 1H), 7.11 (d, J = 6.9 Hz, 1H), 4.32 (s, 2H), 4.13 (s, 2H), 4.00 (s, 2H), 3.87 (s, 2H), 3.56- 3.24 (m, 9H), 2.78 (s, 3H), 2.15 (s, 3H). LC/MS (ESI, m/z): 477.2409 $[M+H]^+$.

*N-(3-(2-Aminoethoxy)-4-methylphenyl)-4-((4-methylpiperazin-1-yl)methyl)-3-(trifluoromethyl)benzamide trihydrochloride (**44d**).* Yield (two-step) 62%. ^{1}H NMR (400 MHz, DMSO-d_6) δ 10.58 (s, 1H), 8.39 (s, 5H), 8.24 (s, 1H), 7.54 (s, 1H), 7.38 (s, 1H), 7.15 (s, 1H),

4.20 (s, 4H), 3.52 - 3.11 (m, 12H), 2.79 (s, 3H), 2.21 (s, 3H). LC/MS (ESI, m/z): 451.2231 $[M+H]^+$.

*N-(4-Chloro-3-(piperidin-4-yloxy)phenyl)-4-((4-methylpiperazin-1-yl)methyl)-3-(trifluoromethyl)benzamide (**44e**).* Yield (two-step) 73%. ^{1}H NMR (400 MHz, DMSO-d_6) δ 11.22 (s, 1H), 10.80 (s, 1H), 9.18 (s, 2H), 8.41 (s, 1H), 8.34 (s, 1H), 8.10 (s, 1H), 7.85 (s, 1H), 7.50 (s, 1H), 7.46 (s, 1H), 4.68 (s, 1H), 4.00 (s, 2H), 3.44 (s, 2H), 3.17 (d, J = 25.5 Hz, 8H), 2.77 (s, 5H), 2.18 (s, 2H), 1.98 (s, 2H). LC/MS (ESI, m/z): 511.2016 $[M+H]^+$.

*N-(4-Methoxy-3-(piperidin-4-yloxy)phenyl)-4-((4-methylpiperazin-1-yl)methyl)-3-(trifluoromethyl)benzamide trihydrochloride (**44f**).* Yield (two-step) 73%. ^{1}H NMR (400 MHz, DMSO-d_6) δ 10.53 (s, 1H), 9.12 (s, 2H), 8.36 - 8.20 (m, 3H), 7.57 (s, 1H), 7.40 (s, 1H), 7.01 (d, J = 6.3 Hz, 1H), 4.47 (s, 1H), 4.22 (s, 2H), 3.87 - 2.68 (m, 18H), 2.09 (s, 2H), 1.88 (s, 2H). LC/MS (ESI, m/z): 507.2513 $[M+H]^+$.

(4-(5-Amino-2-methylphenoxy)piperidin-1-yl)(pyridin-3-yl)methanone (***44g***). To a solution of nicotinic acid (3 mmol, 369 mg) and **42g** (3 mmol, 816 mg) in DMF (15 mL) was added HATU (3.6 mmol, 1.37 g) and DIPEA (4.5 mmol, 585 mg). The resulting mixture was stirred at room temperature for 2 h and the system was quenched with water, extracted with EtOAc and dried with anhydrous Na_2SO_4. The solvents were removed under vacuum to provide the crude product **43g**, which was directly dissolved in EtOAc (20 mL) and Pd/C (5%) was added. The mixture was stirred under hydrogen balloon at room temperature for 6 h. The system was filtered through diatomaceous earth and the filtrate was concentrated under vacuum to give the product **44g** (727 mg, two-step yield 78%) as a yellow oil. ^{1}H NMR (400 MHz, DMSO-d_6) δ 8.65 (s, 2H), 7.88 (d, J = 7.5 Hz, 1H), 7.49 (dd, J = 7.5, 4.7 Hz, 1H), 6.77 (d, J = 7.8 Hz, 1H), 6.28 (s, 1H), 6.09 (d, J =

7.6 Hz, 1H), 4.87 (s, 2H), 4.49 (s, 1H), 3.96 - 3.38 (m, 4H), 2.02 (s, 5H), 1.72 (s, 3H). LC/MS (ESI, m/z): 312.1640 $[M+H]^+$.

BaF3 Isogenic Cell Generation. Retroviral constructs for fusion kinases were made based on the pMSCVpuro (Clontech) backbone. For TEL fusion vectors, the first 1 kb of human TEL gene with an artificial myristoylation sequence (MGCGCSSHPEDD) was cloned into pMSCVpuro retroviral vector, followed by a 3xFLAG tag sequence and a stop codon; for BCR fusion vectors, the first 2.8 kb coding region of p210 amplified from K562 cell line was used in fusion constructs. Then the kinase domain coding sequences were inserted in-frame between TEL/BCR and 3xFLAG sequences. All mutagenesis were performed using the QuikChange Site-Directed Mutagenesis Kit (Stratagene) following the manufacturer's instructions. Retrovirus was packaged in HEK293T cells by transfecting kinase-fusion MSCV vectors together with two helper plasmids, virus supernatants were harvested 48 h after transfection and filtered before infection. Then BaF3 cells were infected with harvested virus supernatants using spinoculation protocol and stable cell lines were obtained by puromycin selection for 48 h. A second selection in the absence of IL-3 was performed to obtain IL-3 independent cell lines that solely depend on the introduced kinase activities for cell proliferation.

Cell Lines and Cell Culture. The K562 (CML), KU812 (CML), MEG-01 (CML), MV4-11 (AML), MOLM14 (AML), U937 (AML), REC-1 (human B-cell lymphoma cell), HL-60 (Human promyelocytic leukemia cells), MEC-1(CLL), CHL (Hamster lung cell), CHO (Hamster ovary cell) cell lines were obtained from American Type Culture Collection (Manassas, VA). The human GIST-T1, GIST882, GSIT48B cells were kindly provided by the Group of Professor Jonathan A. Fletcher, Brigham and Women's Hospital in Boston, USA. All the cells were grown in a humidified incubator (Thermo, USA) at 37 °C under 5% CO_2. GIST-T1, CHO cells were

maintained in DMEM supplemented with 10% FBS, 1% penicillin/streptomycin. GIST-882 and GIST-48B were grown in IMDM supplemented with 10% FBS, 1% penicillin/streptomycin. All the other cell lines and all the isogenic Ba/F3 cells were grown in Roswell Park Memorial Institute (RPMI) 1640 medium supported with 10% FBS, and 1% penicillin/streptomycin. Adherent cells were grown in tissue culture flasks until they were 85-95% confluent prior to use. For suspension cells, cells were collected by spin down at 800 rpm/min for 5 min before use.

ABL1 and c-KIT Protein Purification. A construct encoding c-ABL residues 229-500 with a His tag was cloned into baculovirus expression vector pFASTHTA. The protein was expressed by infecting SF9 cells with high titer viral stocks for 48 h. Cells were harvested and lysed in 30 mM Tris pH7.4, 150 mM NaCl, 3 mM KCl, 10% glycerol, 1 mM PMSF, 2 mM TCEP, 1 mM ADP, 20 mM Imidazole. The supernatant was loaded to Ni-NTA Column (QIAGEN, 1018244). Then the proteins were gradient washed using the same buffer with 50 mM, 100 mM imidazole, then the ABL protein was eluted with Elution buffer (20 mM Tris, 500 mM NaCl, 1% glycerol, 1mM TCEP, 0.5mM ADP, 300 mM Imidazole, pH 8.0). The eluted protein was loaded on desalt column PD-10(GE) to change the buffer to 20 mM Tris, 500 mM NaCl, 1% glycerol, 2 mM TCEP, pH 8.0. The protein was concentrated to 1mg/ml and aliquots were frozen and stored at -80 $^{\circ}$C.

Kinase Biochemical Assay. The fluorescence resonance energy transfer-based Z′-LYTE kinase assay (Invitrogen, USA) was used to evaluate the IC_{50} value of **34** and Imatinib for inhibition of ABL and KIT kinase. The reaction was performed on a 384-well plate with a 10 μL reaction volume per well containing 2 μM peptide (Tyr 02 peptide for ABL kinase, Tyr 06 peptide for KIT kinase) substrate in reaction buffer, and ABL kinase (2.5 μL, 5 ng) or KIT kinase (2.5 μL, 10 ng) with a serial 3-fold dilution of **34** and Imatinib (2.5 μL, 10 μM to 1.5 nM).

The final reaction concentration of ATP was 300 μM. After 1 h incubation, a reaction was developed and terminated, and the fluorescence measured with an automated plate reader (SpectraMax I3, USA). A dose-response curve was fitted using Prism 5.0 (GraphPad Software Inc., San Diego, CA).

Anti-Proliferation Assays. A density of 1 to 2.5×104 cells/mL cells were mixed with various concentrations of compounds then 100 μL was added to each well and incubated for 72 h. Cell viability was determined using the CellTiter-Glo (Promega, USA) or CCK-8 (Beboy, China). Both assays were performed according to the manufacturer instructions. For CellTiter-Glo assay, luminescence was determined in a multi-label reader (Envision, PerkinElmer, USA). For CCK-8 assay, absorbance was measured in a microplate reader (iMARK, Bio-Rad, USA) at 450 nm and 655 nm. Data were normalized to control group (DMSO-d_6). GI_{50} were calculated using Prism 6.0 (GraphPad Software, San Diego, CA).

Signaling Pathway Study. K562, KU812, MEG-01, GIST-T1, GIST-882 and GIST-48B cells were treated with DMSO, serially diluted compound 34, 1 μM Imatinib for 2 h before immunoblotting. For immunoblotting, cells were washed with ice cold phosphate buffered saline (PBS), lysed using radio-immunoprecipitation (RIPA) buffer [150mM NaCl, 1% (vol/vol) Nonidet P-40, 0.5% (wt/vol) sodium deoxycholate, 0.1% (wt/vol) SDS] in 50mM Tris HCl (pH8.0) supplemented with protease and phosphatase inhibitors (Thermo, USA; 1862209). Protein concentrations were determined using the BCA Protein Assay kit (Beyotime, China; P0012) according to the manufacturer's protocol. Proteins were separated by SDS-PAGE and transferred to an Immobilon-P PVDF membrane (Millipore, USA; IPVH00010), and blocked in 5% dry milk in Tris Buffered Saline, with Tween 20 (TBST). Membranes were incubated with primary and secondary antibodies, and target proteins were detected with ECL detection reagent

(Pierce, USA; 32106). β-Actin (A5316) from Sigma-Aldrich was served as a loading control. Rabbit polyclonal antibodies to phospho-KIT Y823 was from Invitrogen (44-498G). Phospho-c-Abl (Tyr245)(73E5) Rabbit mAb (2868), c-Abl antibody (2862), STAT5 (3H7) Rabbit mAb (9358), Phospho-STAT5 (Tyr694)(C71E5) Rabbit mAb (9314), Akt (pan)(C67E7) Rabbit mAb (4691), Phospho-Akt (Thr308) (244F9) Rabbit mAb (4056), Phospho-Akt (Ser473) (D9E) XP® Rabbit mAb (4060), Phospho-Crkl (Tyr207) antibody (3181), Crkl (32H4) Mouse mAb (3182), Phospho-p44/42 MAPK (Erk1/2) (Thr202/Tyr204) (197G2) Rabbit mAb (4377), p44/42 MAPK (Erk1/2) (137F5) Rabbit mAb (4695) antibodies, total c-KIT (3308), phospho-KIT Y719 (3391) , phospho-KIT Y703 (3073), phospho-Stat3 (9145), total Stat3 (12640), phospho-S6K T389 (9206), total S6K (9202), phospho-S6 S235/236 (2211), total S6 (2217), phospho-Src Y416 (6943), total Src (2123) were obtained from Cell Signaling Technology (MA, USA).

Apoptosis Effect Examination. K562, KU812, MEG-01, GIST-T1, GIST-882 and GIST-48B cells were treated with DMSO, serially diluted compound **34**, 1 μM Imatinib for indicated periods. Cells were collected and analyzed by Western blotting using following antibodies: PARP(9532), Caspase-3(9665) from Cell Signaling Technology(MA, USA). β-Actin (A5316) served as a loading control.

Cell Cycle Analysis. K562, KU812, MEG-01, GIST-T1, GIST-882 and GIST-48B cells were treated with serially diluted **34** for indicated periods. The cells were fixed in 70% cold ethanol and incubated at −20 °C overnight, then stained with PI/RNase staining buffer (BD Pharmingen). Flow cytometry was performed using a FACS Calibur (BD), and results were analyzed by ModFit software.

In Vivo Pharmacokinetics Study. Compound **34** was dissolved in 55% saline containing 5% DMSO-d_6 and 40% PEG400 by vortex. The final concentration of the stock solution was 1

mg/mL for administration. Six-eight weeks old male Sprague-Dawely rats were fasted overnight before starting drug treatment via intravenous and oral administration. Animal blood collection time points were as follows: for group 1, 3, 5 (intravenous): 1 min, 5 min, 15 min, 30 min, 1 h, 2 h, 4 h, 6 h, 8 h before and after administration was selected; for group 2, 4, 6 (oral): 5 min, 15 min, 30 min, 1 h, 2 h, 4 h, 6 h, 8 h and 24 h before and after dosing. Each time about 0.2 mL blood was collected through the jugular vein adding heparin for anticoagulation and kept on ice. Then plasma was separated by centrifugation at 8000 rpm for 6 minutes at 2-8 °C. The obtained plasma was stored at -80 °C before analysis. After finishing the test, all surviving animals will be transferred to the repository or euthanasia (CO_2 asphyxiation).

GIST-T1 Xenograft Tumor Model. Six weeks old female nu/nu mice were purchased from the Shanghai Experimental Center, Chinese Academy of Sciences (Shanghai, China). All animals were maintained in a specific pathogen-free facility and used according to the animal care regulations of Hefei Institutes of Physical Science, Chinese Academy of Sciences (Hefei, China), and all efforts were made to minimize animal suffering. To obtain orthotopic xenograft of human mammary tumor in the mice, cells were harvested during exponential growth. Five million GIST-T1 cells in PBS were suspended in a 1:1 mixture with Matrigel (BD Biosciences) and injected into the subcutaneous space on the right flank of nu/nu mice. Daily oral administration was initiated when GIST-T1 tumors had reached a size of 100 to 200 mm^3. Animals were then randomized into treatment groups of 5 mice each for efficacy studies. Compound **34** was delivered daily in a HKI solution (0.5% Methocellulose/0.4% Tween80 in ddH_2O) by orally gavages. A range of doses of **34** or its vehicle was administered, as indicated in figure 9 legends. Body weight and tumor growth was measured daily after **34** treatment. Tumor volumes were calculated as follows: tumor volume (mm^3)＝[(W^2× L)/2] in which width (W) is

defined as the smaller of the two measurements and length(L) is defined as the larger of the two measurements.

K562 Xenograft Tumor Model. Five weeks old female nu/nu mice were purchased from the Shanghai Experimental Center, Chinese Science Academy (Shanghai, China). All animals were housed in a specific pathogen-free facility and used according to the animal care regulations of Hefei Institutes of Physical Science Chinese Academy of Sciences. Prior to implantation, cells were harvested during exponential growth. Ten million K562 cells in PBS were formulated as a 1:1 mixture with Matrigel (BD Biosciences) and injected into the subcutaneous space on the right flank of nu/nu mice. Daily oral administration was initiated when K562 tumors had reached a size of 200 to 400 mm^3. Animals were then randomized into treatment groups of 4 or 5 mice each for efficacy studies. **34** was delivered daily in a HKI solution (0.5% Methocellulose/0.4% Tween80 in ddH_2O) by orally gavage. A range of doses of **34** or its vehicle were administered, as indicated in figure legends. Body weight and tumor growth was measured daily after **34** treatment. Tumor volumes were calculated as follows: tumor volume (mm^3)$=[(W^2 \times L)/2]$ in which width (W) is defined as the smaller of the two measurements and length (L) is defined as the larger of the two measurements.

Immunohistochemistry Stain. Tumor tissues were fixed in 10% neutral-buffered formalin and embedded in paraffin. Six-micron tissue section were prepared, deparaffinized, dehydrated, and then stained with hematoxylin and eosin (H&E) using routine methods. Commercially available primary antibody to human Ki-67 (ZSGB-BIO, Beijing, China) was used for Ki-67 staining. After heat-induced antigen retrieval, formalin-fixed and paraffin-embedded tumor tissue sections were stained with primary antibody overnight at 4 °C. The slides were subsequently incubated with ImmPRES anti-mouse Ig (Vector Laboratories, Burlingame, CA) at

room temperature for 30 min, stained with peroxidase substrate 3,3'-diaminobenzidine chromogen (Vector Laboratories), and finally counterstained with hematoxylin. TUNEL staining was assessed using In Situ Cell Death Detection Kit (POD) (Roche, Mannheim, Germany) according to the manufacturer's instructions.

Molecular Modeling. Molecular docking of compound **34** to the ABL1 kinase and the c-KIT kinase were performed with software Yeti^X 8.3.[19] The kinase domain of chain A in the PDB were used for docking (PDB ID: 5HU9 and 1T46 for ABL1 and c-KIT, respectively). Alternative conformations of the side chains were manually confirmed, and missing side chains were automatically added using AmberTools. The protonation and tautomeric state at physiological pH were confirmed by software Reduce[20] and the receptor side-chain structure was further optimized using Yeti^X 8.3. Compound **34** was constructed using Bio^X 4.6[21] and the atomic partial charges were calculated by AmberTools. Template-based induced-fit docking of small molecules to the two kinases: ABL1 and c-KIT were performed using Yeti^X 8.3. The docked modes were optimized by the directional *Yeti* force field.[22]

NOTES

Dr. Shanchun Zhang is a shareholder of Hefei Cosource Medicine Technology Co. LTD.

ACKNOWLEDGMENTS

Q.L. is supported by the Joint Funds of Research on Major Science Facilities, Key Program of the National NSFC (#U1432250) and the CAS/SAFEA international partnership program for creative research teams. J.L. is supported by the "Personalized Medicines——Molecular Signature-based Drug Discovery and Development", Strategic Priority Research Program of the Chinese Academy of Sciences (Grant No. XDA12020308) and the National Program for Support

of Top-notch Young Professionals. W.W., J.L. and Q.L. are supported by the "Cross-disciplinary Collaborative Teams Program for Science, Technology and Innovation (2014-2016)" of Chinese Academy of Sciences. We are grateful for the China "Thousand Talents Program" support for Q.L. and "Hundred Talents Program" of the Chinese Academy of Sciences support for J.L. and W.W..

ABBREVIATIONS USED

BCR-ABL, breakpoint cluster region - Abelson murine leukemia viral oncogene; KIT, v-kit Hardy−Zuckerman 4 feline sarcoma viral oncogene homolog; CML, chronic myelogenous leukemia; GISTs, gastrointestinal stromal tumors; BLK, B lymphocyte kinase; CSF1R, colony stimulating factor 1 receptor; DDR1/2, discoidin domain receptor 1/2; LCK, lymphocyte-specific protein tyrosine kinase; LOK, lymphocyte oriented kinase; PDGFR, platelet-derived growth factor receptor; TUNEL, terminal deoxynucleotidyl transferase dUTP nick end labeling.

ASSOCIATED CONTENT

Supporting Information

The supporting information is available free of charge on the ACS Publication website at http://pubs.acs.org.

Table S1 listing the DiscoveRx's KINOMEscan selectivity profiling data of compound **34**.

AUTHOR INFORMATION

Corresponding Authors

*Phone: 86-551-65595161. E-mail: qsliu97@hmfl.ac.cn.

*Phone: 86-551-65593186. E-mail: jingliu@hmfl.ac.cn.

AUTHOR CONTRIBUTIONS

The manuscript was written through contributions of all authors. All authors have given approval to the final version of the manuscript. Q.W., F.L., B.W., F.Z. contributed equally to this work.

REFERENCES

(1) Schindler, T.; Bornmann, W.; Pellicena, P.; Miller, W. T.; Clarkson, B.; Kuriyan, J. Structural mechanism for STI-571 inhibition of abelson tyrosine kinase. *Science* **2000**, *289*, 1938-1942.

(2) Simard, J. R.; Getlik, M.; Grutter, C.; Pawar, V.; Wulfert, S.; Rabiller, M.; Rauh, D. Development of a fluorescent-tagged kinase assay system for the detection and characterization of allosteric kinase inhibitors. *J. Am. Chem. Soc.* **2009**, *131*, 13286-13296.

(3) Weisberg, E.; Manley, P. W.; Breitenstein, W.; Bruggen, J.; Cowan-Jacob, S. W.; Ray, A.; Huntly, B.; Fabbro, D.; Fendrich, G.; Hall-Meyers, E.; Kung, A. L.; Mestan, J.; Daley, G. Q.; Callahan, L.; Catley, L.; Cavazza, C.; Azam, M.; Neuberg, D.; Wright, R. D.; Gilliland, D. G.; Griffin, J. D. Characterization of AMN107, a selective inhibitor of native and mutant Bcr-Abl. *Cancer Cell* **2005**, *7*, 129-141.

(4) Wilhelm, S. M.; Dumas, J.; Adnane, L.; Lynch, M.; Carter, C. A.; Schutz, G.; Thierauch, K. H.; Zopf, D. Regorafenib (BAY 73-4506): a new oral multikinase inhibitor of angiogenic, stromal and oncogenic receptor tyrosine kinases with potent preclinical antitumor activity. *Int. J. Cancer* **2011**, *129*, 245-255.

(5) You, W. K.; Sennino, B.; Williamson, C. W.; Falcón, B.; Hashizume, H.; Yao, L. C.; Aftab, D. T.; Mcdonald, D. M. VEGF and c-Met blockade amplify angiogenesis inhibition in pancreatic islet cancer. *Cancer Res.* **2011**, *71*, 4758-4768.

(6) Zhou, T.; Commodore, L.; Huang, W. S.; Wang, Y.; Thomas, M.; Keats, J.; Xu, Q.; Rivera,

V. M.; Shakespeare, W. C.; Clackson, T.; Dalgarno, D. C.; Zhu, X. Structural mechanism of the Pan-BCR-ABL inhibitor ponatinib (AP24534): lessons for overcoming kinase inhibitor resistance. *Chem. Biol. Drug Des.* **2011**, *77*, 1-11.

(7) Okamoto, K.; Ikemori-Kawada, M.; Jestel, A.; von Konig, K.; Funahashi, Y.; Matsushima, T.; Tsuruoka, A.; Inoue, A.; Matsui, J. Distinct binding mode of multikinase inhibitor lenvatinib revealed by biochemical characterization. *ACS Med. Chem. Lett.* **2015**, *6*, 89-94.

(8) Wu, P.; Nielsen, T. E.; Clausen, M. H. FDA-approved small-molecule kinase inhibitors. *Trends Pharmacol. Sci.* **2015**, *36*, 422-439.

(9) Zhao, Z.; Wu, H.; Wang, L.; Liu, Y.; Knapp, S.; Liu, Q.; Gray, N. S. Exploration of type II binding mode: a privileged approach for kinase inhibitor focused drug discovery? *ACS Chem. Biol.* **2014**, *9*, 1230-1241.

(10) Dong, J.; Zhao, H.; Zhou, T.; Spiliotopoulos, D.; Rajendran, C.; Li, X. D.; Huang, D.; Caflisch, A. Structural analysis of the binding of type I, I1/2, and II Inhibitors to Eph tyrosine kinases. *ACS Med. Chem. Lett.* **2015**, *6*, 79-83.

(11) Nagashima, K.; Shumway, S. D.; Sathyanarayanan, S.; Chen, A. H.; Dolinski, B.; Xu, Y.; Keilhack, H.; Nguyen, T.; Wiznerowicz, M.; Li, L.; Lutterbach, B. A.; Chi, A.; Paweletz, C.; Allison, T.; Yan, Y.; Munshi, S. K.; Klippel, A.; Kraus, M.; Bobkova, E. V.; Deshmukh, S.; Xu, Z.; Mueller, U.; Szewczak, A. A.; Pan, B. S.; Richon, V.; Pollock, R.; Blume-Jensen, P.; Northrup, A.; Andersen, J. N. Genetic and pharmacological inhibition of PDK1 in cancer cells: characterization of a selective allosteric kinase inhibitor. *J. Biol. Chem.* **2011**, *286*, 6433-6448.

(12) Kim, H. G.; Tan, L.; Weisberg, E. L.; Liu, F.; Canning, P.; Choi, H. G.; Ezell, S. A.; Wu, H.; Zhao, Z.; Wang, J.; Mandinova, A.; Griffin, J. D.; Bullock, A. N.; Liu, Q.; Lee, S. W.; Gray, N. S. Discovery of a potent and selective DDR1 receptor tyrosine kinase inhibitor. *ACS Chem.*

Biol. **2013**, *8*, 2145-2150.

(13) Liu, F.; Wang, B.; Wang, Q.; Qi, Z.; Chen, C.; Kong, L.-L.; Chen, J.-Y.; Liu, X.; Wang, A.; Hu, C.; Wang, W.; Wang, H.; Wu, F.; Ruan, Y.; Qi, S.; Liu, J.; Zou, F.; Hu, Z.; Wang, W.; Wang, L.; Zhang, S.; Yun, C.-H.; Zhai, Z.; Liu, J.; Liu, Q. Discovery and characterization of a novel potent type II native and mutant BCR-ABL inhibitor (CHMFL-074) for Chronic Myeloid Leukemia (CML). *Oncotarget* **2016**, doi: 10.18632/oncotarget.10037.

(14) Fabian, M. A.; Rd, B. W.; Treiber, D. K.; Atteridge, C. E.; Azimioara, M. D.; Benedetti, M. G.; Carter, T. A.; Ciceri, P.; Edeen, P. T.; Floyd, M. A small molecule-kinase interaction map for clinical kinase inhibitors. *Nat. Biotechnol.* **2005**, *23*, 329-336.

(15) Williams, L. T. Signal transduction by the platelet-derived growth factor receptor. *Nature* **1994**, *367*, 474-476.

(16) Torres, K. E.; Zhu, Q. S.; Bill, K.; Lopez, G.; Ghadimi, M. P.; Xie, X.; Young, E. D.; Liu, J.; Nguyen, T.; Bolshakov, S. Activated MET is a molecular prognosticator and potential therapeutic target for malignant peripheral nerve sheath tumors. *Clin. Cancer Res.* **2011**, *17*, 3943-3955.

(17) Valiathan, R. R.; Marco, M.; Leitinger, B.; Kleer, C. G.; Fridman, R. Discoidin domain receptor tyrosine kinases: new players in cancer progression. *Cancer Metast. Rev.* **2012**, *31*, 295-321.

(18). Pollard, J. W. Trophic macrophages in development and disease. *Nat. Rev. Immunol.* **2009**, *9*, 259-270.

(19) Gianluca, R.; Beat, E.; Martin, S.; Morena, S.; Angelo, V. Probing small-molecule binding to cytochrome P450 2D6 and 2C9: an in silico protocol for generating toxicity alerts. *Chemmedchem.* **2010**, *5*, 2088-2101.

(20) Word, J. M.; Lovell, S. C.; Richardson, J. S.; Richardson, D. C. Asparagine and glutamine: using hydrogen atom contacts in the choice of side-chain amide orientation 1. *J. Mol. Biol.* **1999**, *285*, 1735-1747.

(21) Dobler, M. BioX, a versatile molecular-modeling software; Biographics Laboratory 3R: Basel, Switzerland, **2012**, http://www.biograf.ch/index.php?id=software (Updated Nov 8, 2014).

(22) Vedani, A.; Huhta, D. W. A new force field for modeling metalloproteins. *J. Am. Chem. Soc.* **2002**, *112*, 4759-4767.

Table of Contents Graphic

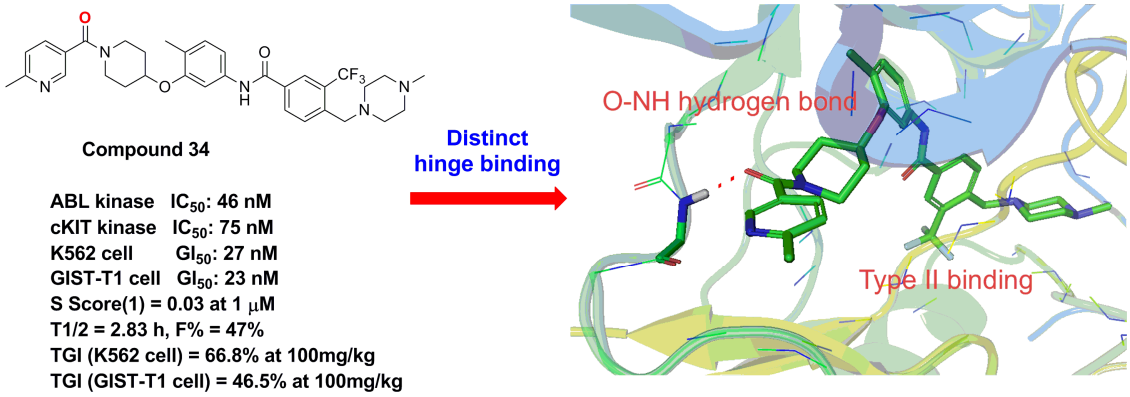

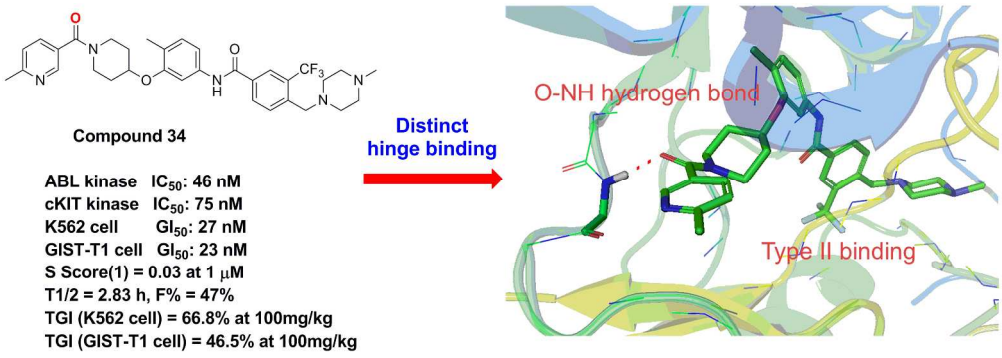

248x87mm (300 x 300 DPI)